Thesis

Morphological description of the human oral mucosa -

Focus on the mechanical properties of the mandibular part

submitted by

Carolina Radetzky

in partial fulfillment of the requirements for the degree of

Doktorin der Zahnmedizin

(Dr^{in}. med. dent.)

at the

Medical University of Graz

executed at the

Division of Macroscopic and Clinical Anatomy

under the supervision of

Sen. Lecture Priv.-Doz. Dr. med. Dent. **Veronica Alexandra Antipova**

Univ.-Prof. Dr. med habil. **Niels Hammer**

Univ.-Prof. Dr. med. univ. Dr. med. dent. **Norbert Jakse**

Graz, 22 July 2024

Declaration of Academic Integrity

I hereby confirm that the present diploma thesis is the result of my own independent scholarly work. I also confirm that in all cases, where material from the work of others (in books, articles, essays, dissertations, and on the internet) is acknowledged, quotations and paraphrases are clearly indicated. No material other than that cited in the reference list has been used. I have read and understood the Medical University's regulations and procedures concerning plagiarism.

Graz, 22 July 2024 Carolina Radetzky m.p.

Acknowledgement

I would like to take this opportunity to express my sincere gratitude to the individuals who have supported and inspired me throughout the creation of this thesis.

First and foremost, I extend my deepest thanks to my supervisor, Sen. Lecture Priv.-Doz. Dr. med. dent. **Antipova, Veronica Alexandra**, for her invaluable guidance, patience, and unwavering support throughout the entire research process. Her expert advice and constructive feedback have significantly contributed to the realization of this work's full potential.

A special thanks also goes to my co-supervisors, Univ.-Prof. Dr. med habil. **Hammer, Niels** and Univ.-Prof. Dr. med. univ. Dr. med. dent. **Jakse, Norbert,** for their valuable insights and suggestions. Their feedback and encouragement have helped me give my best to achieve the set objectives.

Furthermore, I would like to thank Dr. **Haspinger, Daniel** and Dr. **Niestrawska, Justyna A.** for their technical support and expertise during data collection and analysis. Their assistance was indispensable and contributed to the smooth progress of the research.

I am also grateful for the assistance provided by Dr. **Siwetz, Martin** for retrieving the human donor samples.

Additionally, I would like to express my gratitude to my partner in crime **Otto, Sabine**. Her constant companionship, encouragement, and unwavering belief in our abilities have significantly contributed to our success. The camaraderie we shared has not only made the journey enjoyable but also unforgettable. During challenging times, her support has been an invaluable source of strength upon which I could always rely.

Lastly, I want to express my gratitude to my family and friends who have encouraged and supported me during this challenging time. Your unwavering belief in me and your encouraging words have provided me with the necessary motivation to successfully complete this thesis.

Abstract in German

Hintergrund

Das Gewebe der Mundschleimhaut ist verschiedensten Kräften ausgesetzt, insbesondere während des Kauaktes. Unter den Kaukräften unterliegen die oralen Weichteile einer erheblichen elastischen Verformung. Die vorliegende Studie befasst sich mit den biomechanischen Eigenschaften der Mundschleimhaut des menschlichen Unterkiefers im unfixierten Zustand. Die Studie untersucht biomechanische Parameter von chemisch unbehandelten menschlichen Proben der Gingiva im Vergleich zur beweglichen Mundschleimhaut. Frühere Studien konnten zeigen, dass Unterschiede in der Elastizität und Mobilität im Bereich der befestigten Gingiva und der beweglichen Mundschleimhaut bestehen. Es wird ein höheres E-Modul der befestigten Gingiva im Vergleich zur beweglichen Mundschleimhaut erwartet. Dies wurde bisher nur an chemisch fixierten menschlichen Proben getestet.

Material und Methoden

Die Proben wurden mithilfe einachsiger Materialanalysen getestet, durch die mögliche Unterschiede in der Belastbarkeit zwischen der befestigten Gingiva und der alveolären Schleimhaut erhalten werden können. Anschließend wurde das osmotische Stressprotokoll verwendet, um den Wassergehalt im Gewebe zu bestimmen und anzugleichen. Die Gewebeproben wurden nach Vorbelastungszyklen auf Versagen getestet.

Ergebnisse

Die Ergebnisse zeigten, dass die befestigte Gingiva eine höhere Zugfestigkeit (19,4 ± 17,5 MPa) und Steifigkeit aufwies, als die alveoläre Schleimhaut (4,8 ± 3,3 MPa). Der Elastizitätsmodul der befestigten Gingiva war höher als der der bukkalen Schleimhaut. Außerdem zeigten die Cauchy-Spannungs-Dehnungs-Diagramme einen signifikant höheren Wert für die befestigte Gingiva der ortsabhängigen Proben. Darüber hinaus wurde eine statistische Signifikanz der Versagensspannung zwischen den Gruppen der befestigten Gingiva und der Alveolarmukosa festgestellt. In beiden Gruppen erreichte die befestigte Gingiva einen höheren Wert als die Alveolarschleimhaut. In keinem der zugehörigen richtungsabhängigen Tests wurde ein Unterschied festgestellt.

Schlussfolgerung

Die Ergebnisse dieser Studie deuten darauf hin, dass Gewebe aus verschiedenen intraoralen Regionen ein unterschiedliches morphologisches und mechanisches Verhalten aufweisen, was in Zukunft durch histologische Analysen bestätigt werden kann. Darüber hinaus können die Ergebnisse dieser Studie für verschiedene klinische Anwendungen im Bereich der menschlichen Mundschleimhaut nützlich sein und als Grundlage für die Erstellung von Hypothesen für weitere Studien dienen. Künftige Experimente könnten auch unter anderen Bedingungen durchgeführt werden, z. B. mit kürzeren Einfrierzeiten und größeren Probenmengen, um die Aussagekraft zu erhöhen und mögliche Messfehler auszuschließen.

Abstract in English

Background

Oral mucosa tissues are exposed to various forces, particularly when chewing. Under such loading, the oral soft tissues are subjected to considerable elastic deformation. This given study assesses the load-deformation properties of the oral mucosa of mandible in unembalmed human specimens. The study investigates the significance of non-fixed human specimens in the area of the attached gingiva compared to the oral mucosa. Previous studies demonstrated that a difference regarding tissue elasticity and mobility in the area of the attached gingiva and the alveolar mucosa exists. A higher elastic-modulus of the attached gingiva compared to alveolar mucosa is expected, but this has so far only been tested on embalmed human specimens.

Materials and Methods

Human oral mucosa tissue samples were tested using uniaxial load-deformation to investigate a potential difference in resistance between attached gingiva and alveolar regions. An osmotic stress protocol was used to determine the water content of the oral mucosa. Tissue samples are tested for failure after the preconditioning cycle with the Ultimate Tensile Strength test.

Results

The results showed that the attached gingiva demonstrated higher tensile strength (19.4 ± 17.5 MPa) and stiffness than alveolar mucosa areas (4.8 ± 3.3 MPa). The elastic modulus of the attached gingiva was higher than that of the buccal mucosa. Furthermore, failure Cauchy stress versus strain plots revealed a significant higher value for the attached gingiva of the location dependent samples. In addition, statistical significance was observed in the failure stress between the attached gingiva and alveolar mucosa groups. In both groups the attached gingiva achieved a higher value in comparison to the alveolar mucosa. No difference was found in any of the related direction dependent sample tests.

Conclusion

The results of this study suggest that tissues from different intraoral regions exhibit different morphological and mechanical behaviours, which may be confirmed by histological analysis in the future. Furthermore, the results of this study may be useful for various clinical applications in the field of human oral mucosa and serve as a basis for hypothesis generation for further studies. Future experiments could also be performed under different conditions, such as shorter freezing times and larger sample sizes.

Publication Disclaimer

Region- and direction-specific mechanical tensile properties of the human oral mucosa

Daniel Ch. Haspinger*, Sabine Otto*, Carolina Radetzky*, Justyna A. Niestrawska, Teresa M. Pirker, Martin Siwetz, Norbert Jakse, Niels Hammer[&], Veronica Antipova[&]

*These authors contributed equally to this work.

[&]These authors contributed equally to this work.

Submitted as an oral presentation, 118. Annual Meeting of the Anatomischen Gesellschaft (Graz, 25.-27.09.2024).

Table of contents

Abbreviations

PEG	Polyethylene glycol
TRIS	Tris(hydroxymethyl)aminomethane
OSP	Osmotic stress protocol
UTS	The Ultimate Tensile Strength
MC	mandible crest
BL	bucco-lingual
Att.	Attached
Alv.	Alveolar
G.	Gingiva

Table of figures

List of tables

1 Introduction

Structural integrity of oral mucosa tissue is an important precondition for overall oral health. Histologically, the oral mucosa consists of multilayered, non-cornified squamous epithelium. Its tissue elasticity also varies dependent on region. The mucogingival line marks the boundary between the attached gingiva, which is firmly adherent, and the alveolar mucosa, which is largely mobile. A previous study confirmed the difference in elasticity and mobility between these two regions. Showing that higher elastic modulus of the attached gingiva compared to the alveolar mucosa is expected, but so far has only been tested on embalmed human specimens [1].

1.1 Anatomy of the mandibular region

The lower jaw (mandible) is a very important and complex bone that is not only used for the basic functional aspects of everyday life, but also holds a significant impact on the aesthetic appearance and the entirety of the human face. There is ongoing research into the anatomy, physiology and pathology of the mandible which is helping to develop a further understanding of the complex structure and multiple functions of the bone. For these reasons, the anatomy of the mandible will be discussed in more detail in this study to provide a basic understanding of the extraction site [2].

1.1.1 Topography of the mandibular region

Overall, the mandible is a central bone attached to the skull which helps to perform a variety of functions. This strong, U-shaped bone forms the lower part of the facial skeleton and consists of two bony arches joined at the front by the chin. The lower jaw is the only movable bone in the skull and plays a crucial role in essential daily activities such as chewing, speaking and swallowing. Shape and structure of the mandible contributes significantly to the aesthetic appearance of a person and is therefore of great interest in dentistry, orthodontics and plastic surgery [2, 3].

1.1.2 Bone structure of the mandibular region

The body of mandible serves as a central bone of the skull, constituting the lower half of the face. Anatomically, the mandible comprises a horizontal body, the base of the mandible

which is forming the chin, and two vertical legs extending upwards. Extending upwards from the mandibular condyles, the vertical legs of the mandible, also known as the ramus of mandible, are divided into two processes, the anterior coronoid process and the posterior condylar process. These processes serve as attachment points for muscles and ligaments controlling mandibular movement [4]. The mandible is connected to the facial skull by the temporomandibular joint, with the mandibular condyle forming the joint head. This joint is located at the end of the ascending branch, the ramus mandible, which merges into the mandibular body [5]. The temporomandibular joint enables the opening and closing of the mouth, along with various movements of the lower jaw during speaking and chewing. The teeth are anchored by the base of the lower jaw, which contains the dental compartments (alveolar juga). These compartments are arranged along the upper part of the body, not only securing the teeth in place but also maintaining the rows of teeth and ensuring functional bite guidance [3, 4]. The trigeminal nerve passes through the mental foramen. The position of this hole is clinically important, as the pressure sensitivity of the nerve can be tested here [5]. The mandibular foramen is located on the medial side of the mandibular ramus, which serves as a passage for nerves and blood vessels supplying the lower jaw [3, 4].

1.1.3 Muscles of the mandibular region

A complex set of muscles controls the movement of the lower jaw. Notable among these are the masseter, temporalis, medial pterygoid, and lateral pterygoid muscles. The masseter, which extends from the zygomatic arch to the mandible, is considered to be the strongest muscle in the jaw and is primarily responsible for closing the mouth. Meanwhile, the temporalis muscle, located in the temporal region, also orchestrates the closing of the lower jaw. Composed of two components, the pterygoid muscle includes the medial and lateral pterygoid [6]. The lateral pterygoid muscle initiates the opening of the mouth, which is then continued by the suprahyoid muscles. As the temporomandibular joint opens, fibres of the lateral pterygoid muscle enter the articular disc. This muscle is considered to be the primary guiding muscle of the temporomandibular joint [5]. While the medial pterygoid aids in mouth closure and contributes to chewing, the lateral pterygoid spearheads the task of mouth opening. The harmonious coordination of these muscles supports the complex jaw movements necessary for speech, mastication, and various functions. A profound understanding of the anatomy of these muscles is indispensable for dentists, surgeons, and therapists, ensuring precise treatment of oral and maxillofacial maladies [3, 6].

1.1.4 Arterial and venous blood supply of the lower jaw

The arterial supply to the lower jaw is mainly provided by branches of the maxillary artery, in particular the inferior alveolar artery. This enters the mandible through the mandibular foramen and supplies the teeth and jawbone. At the chin, it emerges from the mental foramen as the mental artery and supplies the chin and lower lip. In addition, the facial artery, another branch of the external carotid artery, supplies the surface structures above the lower jaw, particularly through the submental artery. The lingual artery, which mainly supplies the tongue, also contributes the supply of the floor of the mouth and adjacent structures [3, 7].

Venous drainage is provided by a dense network of veins which usually accompany the arteries. The inferior alveolar vein accompanies the artery of the same name, draining the lower jaw, teeth and lower lip, and flows into the pterygoid plexus, which in turn drains into the maxillary vein. Furthermore, the facial vein drains the superficial structures of the lower jaw, while the mental vein drains the chin and lower lip and eventually joins the internal jugular vein. The lingual vein, which drains the floor of the mouth and adjacent structures, also drains into the internal jugular vein [3].

1.1.5 Innervation of the mandible

The mandibular nerve is the third main branch of the trigeminal nerve (V). It originates from the Gasser ganglion in the skull and runs through the foramen ovale into the mandible. Within the mandible, the mandibular nerve is divided into several branches that innervate different areas of the face and oral cavity. The most important branches of the mandibular nerve include the auriculotemporal nerve, which is responsible for supplying parts of the scalp, and the external auditory canal. It is also comprised of the buccal nerve, which innervates the cheek, the lingual nerve, which supplies the tongue and parts of the oral mucosa, the inferior alveolar nerve, responsible for the sensitivity of the lower teeth, and finally the lower jaw bone and the gums. Through this, complex network of branches, the mandibular nerve ensure precise sensory innervation in the lower jaw and surrounding regions [6].

1.2 Histology of the gingiva

In the domain of oral anatomy, one encounters the mandibular gingiva, also referred to as the oral mucosa of the mandible, safeguarding the tooth-bearing tissue within the mandible.

This unit is divided into three distinct parts, as seen in Figure 1. They are marked by variations in histology, clinical attributes, and functionality. Histologically speaking the gingiva boasts several layers of tissue, with the outermost layer comprising of the gingival epithelium, an epithelial tissue forming a robust barrier against external assailants such as bacteria and mechanical stress. Nestled beneath the gingival epithelium lies the underlying connective tissue, known as the Lamina propria, harbouring a complex network of blood vessels, nerve endings, and assorted immune cells, pivotal in orchestrating defences against infections. In our exploration, we embark on a detailed examination of the contrasting features between the attached gingiva and the alveolar mucosa, visible in Figure 2 [3, 8].

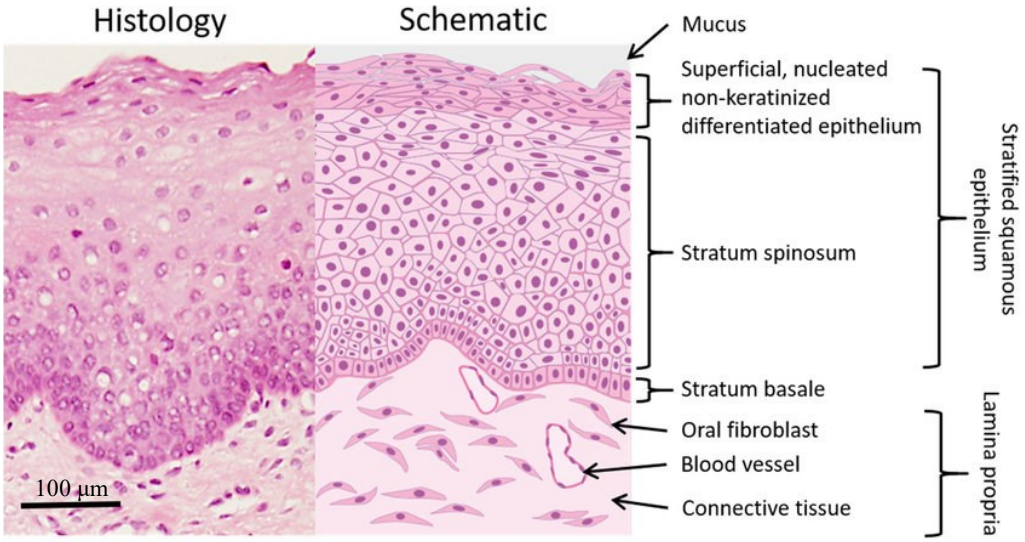

Figure 1: Histological (left) and schematic (right) image of the buccal oral mucosa (histological image courtesy of Prof. Keith Hunter, Unit of Oral Pathology, University of Sheffield). Scale bar = 100 µm [9].

1.2.1 Histological topography of the oral mucosa

The oral mucosa consists of a multi-layered squamous epithelium, which can be keratinised or non-keratinised depending on the region and a connective tissue Lamina propria. This always contains defence cells such as lymphocytes and macrophages. In some areas there is a connective tissue submucosa underneath, in which small salivary glands are embedded. The squamous epithelium regularly contains non-epithelial cells such as melanocytes, dendritic cells and Merkel cells. The oral mucosa is rich in sensory nerve endings, some of

which have a complex structure. Two types of mucous membrane can be distinguished in the alveolar mucosa and the masticatory mucous membrane, as seen in Figure 2 [10].

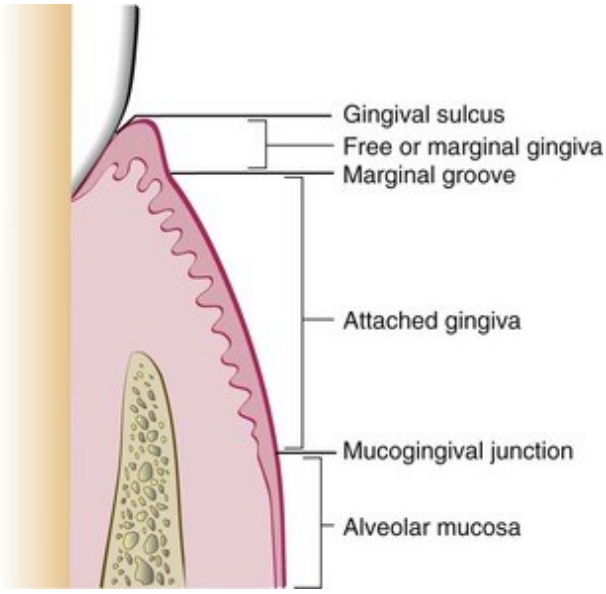

Figure 2: Diagram showing the anatomic landmarks of the gingiva [11].

1.2.2 Alveolar mucosa

The mucogingival line separates the attached gingiva from the alveolar mucosa. On the mobile structures of the mouth, the alveolar mucosa is referred to as the mobile mucosa or lining mucosa and is found on the soft palate, cheeks, lips, floor of the mouth and the vestibular fornix. The epithelium covering the mucosa consists of non-keratinised, stratified squamous epithelium. This is in contrast to the keratinised surface of the attached and free gingiva. Histologically, the gingiva consists of a weakly keratinised, multi-layered squamous epithelium [8].

Beneath the epithelium is a loose Lamina propria, which is less dense and less fibrous than in the attached gingiva. This allows greater mobility of the mucosa. The alveolar mucosa has a clearly pronounced submucosa, which consists of loose connective tissue and contains numerous blood vessels, nerves and fatty tissue [12]. This submucosa is responsible for the mobility of the mucosa. The alveolar mucosa differs from the attached gingiva primarily due to the non-keratinised epithelium, the loose attachment and the clearly pronounced submucosa, which enables its mobility. These differences are decisive for the respective functions and properties of the various areas of the oral mucosa [13].

1.2.3 Masticatory mucous membrane

The masticatory oral mucosa is mainly found in areas that are subjected to high stress during chewing, such as the gums (gingiva) and the hard palate. It is covered with a multi-layered, highly keratinised squamous epithelium that protects against mechanical stress. Beneath the epithelium is a dense Lamina propria, which is rich in collagen fibres to provide additional stability. This mucosa is firmly attached to the underlying bone or tissue, which limits its mobility and increases its resistance. The masticatory oral mucosa plays a crucial role in maintaining oral health and efficient food intake [10].

Spanning a width of 3-9 mm, the gingiva constitutes a strip of tissue that is partially attached to the tooth and partially to the alveolar process. It consists of keratinised squamous epithelium and is considered part of the masticatory oral mucosa. It can be divided into the gingival sulcus, free or marginal gingiva and attached gingiva [14].

1.2.3.1 Gingival sulcus

The gingival sulcus is the narrow gap between the tooth and the adjacent marginal gingiva. It is approximately 1-3 mm deep in healthy conditions and forms the gingival pocket. This area is lined with a non-cornified squamous epithelium, so-called sulcular epithelium. The gingival sulcus plays an important role in the detection and diagnosis of gum diseases, as a depression may indicate inflammation or periodontitis. It acts as a barrier to microbial invasion, with the sulcular epithelium and gingival fluid providing a protective function [14].

1.2.3.2 Marginal gingiva

The marginal gingiva is the part of the gum that surrounds the tooth like a collar and forms the transition to the gum line. It is not firmly attached to the underlying bone and forms the gingival pocket, which acts as a protective barrier against bacterial invasion. Histologically, it consists of a multi-layered keratinised squamous epithelium and a dense Lamina propria. This region contains defence cells such as lymphocytes and macrophages that contribute to immune defence. The marginal gingiva plays an important role in maintaining gum health and preventing periodontal disease [10].

1.2.3.3 Attached gingiva

The keratinized attached gingiva contributes to stabilizing the gingival margin and assists in dispersing the physiological forces exerted by the muscular fibres of the alveolar mucosa on the gingival tissues. It therefore plays a crucial role in enhancing the resistance of the periodontium to external injuries [15].

Extending from the bottom of the gingival crevice to the mucogingival junction, the attached gingiva refers to the gingival portion. Along its edges, it seamlessly connects with the rest of the gingiva. The alveolar periosteum is strong, elastic, and tightly linked to the periosteum beneath it. To determine the attached gingiva's width, one can calculate it by subtracting the sulcus or pocket depth from the distance between the crest of the gingival margin and the mucogingival junction [16].

1.3 Preservation methods

1.3.1 Unfixed human tissue use for biomechanical experiments

Characterizing the mechanical properties of living human oral tissues has been difficult due to ethical concerns and challenges in obtaining tissue samples for testing. Unfixed human donors tissues are scarce for biomechanical testing and degrade quickly, posing a potential infection risk [17]. A study [18] tested the soft tissues around human teeth within an hour of harvesting, using tissues stored in Ringer's solution from only three subjects, without specifying the age or gender of the cadavers. Subsequent studies [12, 19] measured compressive stresses on tissues in living participants using pressure transducers. However, the lack of standardized methodology makes the compressive modulus data unreliable. Additionally, compressive pressure could only be applied until the participants experienced pain, and pain thresholds vary between individuals [1].

1.3.2 Thiel embalming

The original Thiel embalming solution includes specific amounts of 4-Chloro-3-methylphenol (C_7H_7ClO), various nitrite-based salts, along with small quantities of formaldehyde, ethylene glycol for tissue plasticity preservation, boric acid as a

disinfectant, and water [20]. Several adaptations of this mixture have been made by different groups, resulting in satisfactory embalming outcomes [21-23]. Understanding the effects of each Thiel component on biomechanically relevant parameters such as tissue water content and collagen integrity is important [20, 21].

Thiel embalming of human tissues has become a widely accepted method, providing tissues with realistic properties suitable for various anatomical teaching and surgical training purposes across different medical disciplines. The key advantages of Thiel embalming include realistic tissue colour, flexibility, and plasticity [24]. It is seen as a balance between the rapidly deteriorating non-fixated tissue and the long-lasting but biomechanically unsuitable standard embalming techniques, typically based on formaldehyde. Despite the significant acellularization introduced by Thiel embalming [25], the biomechanics of the extracellular matrix are largely preserved, making Thiel-embalmed tissues suitable for fascial research and dissection [26].

However, there is limited research on the effects of Thiel embalming on tissue properties, both in human or animal tissues. Some studies hypothesize that Thiel embalming alters the mechanical properties of human head soft tissues. The findings suggest that Thiel-embalmed tissues may not accurately represent lifelike biomechanical behaviour under quasi-static conditions and this discrepancy may extend to conditions with much higher loading rates due to the viscoelastic nature of extracellular matrix tissues. Thiel-embalmed tissues also exhibit higher variability compared to fresh tissues, likely due to differences in water content, although the extent to which Thiel embalming influences water content remains unclear [27, 28].

Specifically, Thiel embalming effects the elastic behaviour of tissues such as the dura mater, temporalis muscle fascia, and scalp, likely due to dehydration and potential alterations in collagen, which in turn affects the load deformation behaviour of fascial tissues. Additionally, Thiel embalming negatively impacts muscle integrity, rendering these tissues unsuitable for biomechanical testing. Therefore, the use of Thiel-embalmed soft tissues of the head for biomechanical studies should be limited to preliminary orientation tests [26].

1.3.3 Formaldehyde embalming

In anatomy fixation is performed to process tissue specimens, as it helps to preserve cellular architecture, proteins, carbohydrates, and the overall chemical composition. It is also utilized for disinfectant purposes, killing many microorganisms [29]. In the 19th century the physician Ferdinand Blum, native to Frankfurt, discovered the hardening nature of formaldehyde, when the skin on his finger came in contact with the chemical. One major advantage of formaldehyde as fixating agent is the cheap production process of aqueous formaldehyde. Moreover, it is very flexible, as it works under a variety of different conditions and is usable with diverse kinds of tissues. It is not prone to "over fixation", meaning that the tissue does not become hardened unpredictably [30]. Formaldehyde is used as a long-term storage in laboratories as it does not readily decompose [31]. However, the formalin fixation process, while preserving specimens, introduces uncertainties regarding their biomechanical similarity to fresh specimens. Previous reports suggest that formalin-fixed specimens may be stiffer, but quantitative data is lacking. The aim of a previous study [32] was to compare the biomechanical properties of fresh and formalin-fixed spinal specimens, focusing on the L1-2 motion segments of six 16-week-old calf spines. Range of motion and neutral zone were assessed in flexion/extension, left/right axial rotation and right/left lateral flexion. The results showed a significant reduction in range of motion in formalin-fixed specimens, up to 80%, and a reduction in the neutral zone of up to 96% [32].

Despite its importance in industry, formaldehyde exhibits a wide range of harmful effects on the human body, potentially leading to gene mutations, chromosomal defects, and cellular changes. Additionally, it has a significant impact on fertility by altering testicular morphology and reducing sperm count [33]. Recently, formaldehyde has been classified as a carcinogenic compound in category 1B due to its association with various cancers, such as nasopharyngeal cancer through inhalation, as well as skin, blood, and brain cancers [34]. Furthermore, not only environmental exposure to formaldehyde poses health risks, but endogenously produced formaldehyde can also lead to significant health concerns [34, 35].

There is a strong link between formaldehyde exposure and both reproductive and developmental toxicity. Pregnant females exposed to the chemical showed a slightly higher risk of spontaneous abortion and an increased frequency of congenital anomalies

[36]. As a result, formaldehyde has been severely restricted, prompting intense research into alternatives, especially in adhesives [35].

Consequently, this study suggests that formalin-fixed specimens are not a suitable representation of in vivo conditions for biomechanical testing purposes [32].

1.3.4 Mechanical characteristics of human mucosa

The mechanical properties of the basement membrane can be characterized as its cushioning attributes, which provide the ability to withstand compression and tension on a sustained or cyclical basis. The modulus of elasticity, considered a fundamental parameter in defining material behaviour, describes how an object deforms proportionally to the force applied to it. Oral mucosa has been demonstrated to have a high degree of deformation under compression, and the elastic modulus seems to vary widely [37]. The mucosa's stiffness, being a heterogeneous material, is influenced by its solid matrix structure including the epithelial layer, fibrous network, and blood vessels, as well as its fluid components. Previous research on its mechanical properties has used porcine oral mucosa tissues [38, 39]. Several computational modelling studies have attempted to simulate the pressure that complete dentures apply to the oral mucosa and the underlying alveolar bone [37]. However, these studies inaccurately assumed that the elastic modulus and tensile stress of the oral mucosa were uniform across the entire mouth. This misassumption impacts the validity of the finite element analysis (FEA) simulations and the conclusions that can be drawn from these studies [17]. When assessing the feasibility of using cadaveric tissue for measuring mechanical properties, it is important to consider the preservation conditions of post-mortem tissues, including embalming techniques. Commonly used chemicals like glutaraldehyde or formaldehyde aim to prevent tissue deformation and maintain the histological structure of soft tissues. However, it is known that these chemicals alter biomechanical properties by extensively cross-linking the tissues [1].

1.4 Aim of the study

This study uses biomechanical tests to investigate the modulus of elasticity, tensile strength and strain at maximum load using fresh-frozen, unembalmed human tissues of the mandible to observe a potential difference between the alveolar mucosa and the attached gingiva. In

addition, directional dependence of the tissue was observed, mandible crest (MC) and bucco-lingual (BL) directions. The possible difference between attached gingiva and alveolar mucosa will provide information on the loading capacity, but also on tissue anisotropy. Both mechanical and microstructural parameters were then recorded.

The mechanical attributes of the foundational mucosa can be characterized by its cushioning ability, which provide the ability to withstand continuous or cyclic compression and tension. The modulus of elasticity, considered one of the fundamental parameters used to characterize how materials behave, represents the physical tendency of an object to deform in proportion to the traction force. Oral mucosa has been observed to exhibit high deformability under compression, with the elastic modulus showing variation across a wide spectrum. Given its heterogeneous nature, the stiffness of mucosal tissue arises from both its solid matrix structure and its fluid components [1].

Hence, this study aimed to assess the elastic modulus and tensile properties of unembalmed human oral mucosa tissues of two locations at the mandibula in various directions. The null hypothesis stated, that there would be a disparity in the modulus of elasticity and the tensile properties of the tissues of the oral mucosa.

2 Material and Methods

The study was approved by the Ethics Committee of the Medical University of Graz, protocol number 35-500 ex 22/23. The oral mucosa of the lower jaw from 11 individuals were dissected and frozen at -80°C in a post-mortem condition. All body donors were bequeathed to the Division of Macroscopic and Clinical Anatomy of the Medical University of Graz (Austria) under the approval of the ongoing body donation program of the Medical University of Graz and in accordance with the Styrian Death and Funeral Act. The osmotic stress protocol as well as biomechanical testing of the oral mucosa was performed at the Division of Macroscopic and Clinical Anatomy of the Medical University of Graz (Austria). All specimens were preserved by shock-freezing them to -80°C prior to the biomechanical testing and the osmotic stress protocol.

The samples are subjected to various testing methods to detect potential variances in resilience between the attached gingiva and alveolar mucosa. The osmotic stress protocol is employed to evaluate tissue water content, as it is known to influence tissue mechanics. During the preconditioning cycle, all samples undergo a preconditioning procedure consisting of 20 loading/unloading cycles within a force range of 0.5 - 2.0 N. Subsequent to the preconditioning phase, the tissue samples are subjected to testing until failure. Force-displacement measurements were performed at a crosshead displacement rate of 20 mm min^{-1} and a sampling rate of 100 Hz.

2.1 Study population and exclusion criteria

Body donors from the Department of Macroscopic and Clinical Anatomy were dissected between April 2022 and May 2022. Approximately 20 donors were expected, 11body donor samples met the size requirements. Size determination was dictated by the possibility to obtain at least 4 dog-bone shaped samples from the donor specimens. For the body donor collective, no minimum or maximum age, as well as both men and women were included. Furthermore, exclusion criteria were completely edentulous jaws, since the attached gingiva was primarily examined. Specimens with injuries in the mandibular region were not included in the study. Incoming body donations were pseudonymized at the Division of Macroscopic and Clinical Anatomy. It is not possible for the investigators to determine the identity of the donors. Personal data will be kept under lock and key by the chair holder and will not be

part of this study. Biomechanically relevant data such as age, sex, height, weight and, if applicable, cause of death was recorded.

2.2 Retrieval and processing of human oral mucosa

Samples were conducted from a total of 11 specimens. All of the given samples were obtained from two distinct intraoral locations, namely the vestibular and the gingival sites. The collection procedure took place at the Division of Macroscopic and Clinical Anatomy of the Medical University of Graz, where immediate measures were implemented to mark, document, and subsequently shock-freeze the specimens in an -80°C cold freezer for preservation until the testing phase [1].

It is noteworthy, that the 11 specimens provided for the study exhibited partial edentulism in the mandible. Conforming to ISO 527-2 standards (International Standard Organization, 1996). The donors had no history of connective tissue disease and the tissues were collected fresh and without chemical fixation [27].

The incision procedure involved cutting along the marginal gingiva of teeth 45-35, circumventing any partial teeth that remained. Following this, a longitudinal incision was made from cranial to apical, and these incisions were then interconnected. This approach facilitated the removal of both the attached gingiva and the alveolar mucosa in a single sample (Figure 3). In order to ensure the preservation of the tissue for later testing, the samples were shock-frozen at -80°C for storage [1, 27].

Figure 3: Full sample retrieval with attached gingiva and alveolar mucosa, of human body doner.

2.3 Native water content adjustment

While it is recognized that changes in the water content of biological soft tissue impact mechanical characteristics, there has been limited effort to regulate the tissues water content before the biomechanical tests were conducted as part of standardization procedures. This study aimed to explore, how modified water content affects tissue specific mechanical properties. Autopsy-derived samples of attached gingiva and alveolar mucosa were obtained and underwent osmotic adjustments to regulate water content. Macro-mechanical tensile tests, employing video tracking of deformation were conducted. Furthermore, analysis included the modulus of elasticity, tensile strength, and elongation at maximum force. Varied mechanical properties were observed at different water concentrations, emphasizing the necessity to regulate soft tissue water content in the experiment to enhance their validity. The osmotic stress protocol (OSP) offers a practical and dependable standardization method to offset variations in water content influenced by factors like age at death, post-mortem interval, and tissue processing time, known to affect stress-strain properties [40].

Before commencing the actual test series, parts of the samples were tested in three different Polyethylene glycol (PEG) solutions, 2.5 wt%, 5 wt% and 10 wt%, for 8, 12 and 24 hours respectively, in order to achieve an average uniform water content.

2.3.1 Adjusting the sample water content using the osmotic stress technique

The osmotic stress protocol (OSP) was developed to restore the water content in the samples to their original state. Polyethylene glycol (PEG; Rotipuran, Carl Roth GmbH + Co. KG, Karlsruhe, Germany; molecular weight 20.000 Da) was prepared at concentrations ranging from 2.5 wt% to 5 wt% and 10 wt% in an isotonic sodium-chloride solution buffered with 20 mM Tris (hydroxymethyl aminomethane; pH=7). Ten small samples were obtained from each of the eleven body donors, which results in a sample count of 110 samples. One sample per donor was used in the control group. The remaining 9 samples/donor were enclosed in 42-mm dialysis membranes (Carl Roth GmbH + Co. KG, Karlsruhe, Germany; molecular weight cut off = 6000–8000 Da), sealed at both ends (Figure 4a), and immersed in the three PEG solutions already mentioned for durations of 8, 12, and 24 hours at 4 °C under continuous fluid stirring so to facilitate diffusion (Figure 4b, c). Subsequently, the samples were filled in different Eppendorf tubes, which were beforehand weighed with a Quintix® and Secura® precision scale empty, and afterwards the filled Eppendorf tubes were shock-frozen at -80°C for 3 hours. Thereafter, the samples, were filled in their tubes and weighed in a wet state. Following this, the samples were vacuum-dried for 48 hours, and re-weighed in a dry state so to assess their water content. The remaining eleven samples (one sample/donor) served as control samples to establish the initial water content of the oral mucosa in its fresh state [27].

The relative water content in percentage was calculated using the following formula [40]:

$$\phi = \frac{W_{wet} - W_{dry}}{W_{wet}} \quad (1)$$

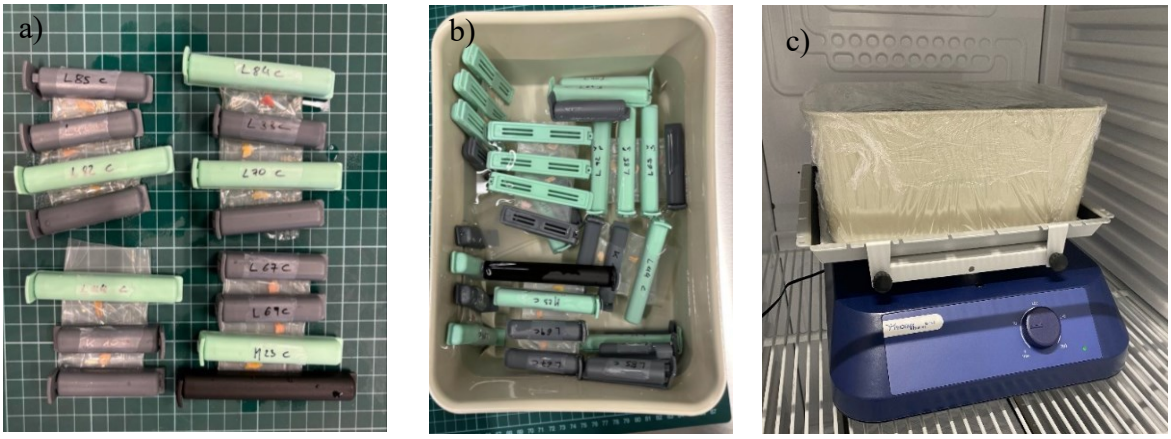

Figure 4:(a) Samples of the OSP clamped in Dialysis membrane, (b) Samples of the OSP in Dialysis membrane submerged in PEG solution, (c) Continuous fluid stirring of the OSP samples in PEG solution with the shaker Phoenix RSOS.

2.3.1.1 Dialysis Membrane

The Spectra/Por® 1 Dialysis Membranes, MWCO 6000 to 8000, by Spectrum® Laboratories, has established itself as the most effective membrane for laboratory dialysis. It lacks any inherent charge and exhibits minimal solute adsorption. Unlike natural cellulose, which is rigid and highly crystalline, regenerated cellulose is predominantly amorphous and swells significantly in water. Nonetheless, it retains small crystalline regions that stabilize the structure, allowing it to maintain integrity. Water-swollen spaces between these regions serve as pores, enabling passage of sufficiently small solute molecules. The gel-like nature of regenerated cellulose makes it susceptible to mechanical strain, potentially altering its porosity [41].

2.3.1.2 Eppendorf Tubes

Eppendorf tubes are a staple in laboratories worldwide, known for their reliability and versatility. These tubes, typically made of polypropylene, are designed to securely contain small volumes of liquids, making them indispensable for various molecular biology and biochemistry applications [42].

In this study the Eppendorf Tubes® 5.0 mL were used for the osmotic stress protocol. For easy identification the Tubes were labelled with waterproof marker, including the sample identification number, percentage of PEG used and duration of exposure to PEG, for facilitating efficient organization in the lab. Initially, small holes had to be drilled in the lids of the tubes to avoid damaging the samples during the vacuum test. All tubes were weighed three times with the help of the Quintix® and Secura® precision scale by Sartorius. With the hole in the lid, the tubes were weighed empty to determine the weight of the samples in the tubes. Each tube contains a sample with a specific PEG concentration and exposure time, so the tubes were weighed a second time with samples after PEG exposure and frozen at -80°C. The third weighing was carried out after the vacuum test to determine different water concentrations.

2.3.1.3 Quintix® and Secura® precision scale

For this study, a Sartorius Quintix® and Secura® precision balance (model 26, 35, 65, 125, 125D, 225D, 324) with a maximum weighing capacity of 310 g was selected to weigh the empty tubes, tubes with samples, and tubes with samples after the vacuum trail. The choice to use this scale was made because of its consistent readings and excellent repeatability, ensured by Sartorius quality and technology developed and design in Germany. For this study, this scale was selected due to its wide array of features [43].

2.3.2 Control group

A control group for the osmotic stress protocol would consist of one sample/donor, treated similarly, but would not be exposed to the osmotic stress conditions. These control samples would undergo the same preparation steps and vacuum drying protocol, but would not be subjected to PEG immersion. The purpose of the control group is to establish a baseline against which the effects observed in the experimental group exposed to osmotic stress are compared. The control group helps to determine whether any observed changes in the experimental group are due to the osmotic stress treatment or to other factors. By including a control group, one can ensure the validity and reliability of the experimental results [40].

2.3.3 Polyethylene glycol (PEG) solution preparation

PEG [%]	PEG [g]	Isotonic solution [ml]	TRIS [g]
2.5	25	1000	2.42
5	50	1000	2.42
10	100	1000	2.42

Table 1: PEG solution preparation

$$20 \cdot 10^{-3}\ mol\ L^{-1} \cdot 1\ L \cdot 121.14\ g\ mol^{-1} = 2.42\ g\ TRIS \qquad (2)$$

2.3.4 Mixing the PEG Solution (5%)

In accordance to literature procedure [27] and seen in Figure 5, first 50 g of PEG powder were dissolved in 1 L distilled water. Then, 2.42 g of Tris(hydroxymethyl)aminomethane (TRIS), was weighed and dissolved it in 1 L distilled water. Thereafter, an isotonic NaCl solution with a concentration of 0.1% was prepared by dissolving 100 ml of NaCl in 1 L water. Then, 100 ml of NaCl solution, 2.42 g of TRIS and 50 g of PEG powder was mixed and then distilled water was added until a volume of about 1 L. The mixture is placed on a magnetic plate and stirred for 20 minutes. Afterwards the pH was adjusted with hydrochloric acid (HCl, 3N). The pH is then checked again, before storing the solution in the refrigerator at a temperature of 4.5 °C.

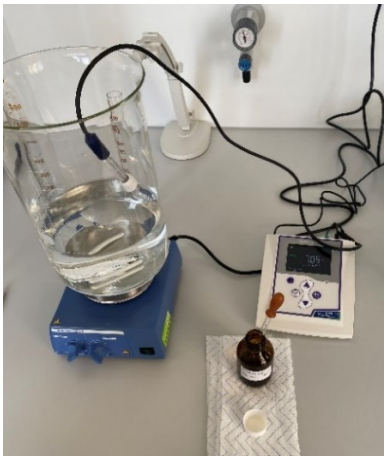

Figure 5: PEG solution production.

2.3.4.1 Polyethylene glycol

Polyethylene glycol (PEG; Rotipuran, Carl Roth GmbH + Co. KG, Karlsruhe, Germany; molecular weight 20.000 Da) can remove water from tissues, especially at higher concentrations or after exposure over a long period of time. This is due to its osmotic properties. PEG with low molecular weight draws water out of cells and tissues because it has a higher osmotic activity compared to the surrounding tissue. This can dehydrate cells and alter their structure. In biochemical or cell culture applications, this property is often used to preserve cells or dehydrate tissue samples, leading to better fixation and preparation. At low concentrations or with short exposure, the effect on tissue hydration may be minimal. However, it's important to consider the concentration and exposure time of PEG to avoid unwanted effects [44].

In this study, the samples were exerted to 8, 12 and 24 hours of submersion in PEG at a concentration of 2.5 wt%, 5 wt%, or 10 wt% PEG, respectively.

2.3.4.2 Tris(hydroxymethyl)aminomethane

Tris(hydroxymethyl)aminomethane (TRIS), is commonly used to maintain the pH of solutions within a specific range. Its buffering capacity and low tendency to form complexes with metal ions make it a preferred choice for many applications in biochemistry and molecular biology. Tris-(hydroxymethyl)-aminomethane has the molecular formula $C_4H_{11}NO_3$ and a molar mass (M) of 121.14 g mol^{-1}. Another advantage of TRIS is its ability to maintain a constant pH environment at constantly changing temperatures. High purity (>99.3%) of the TRIS buffer is crucial to ensure consistency and reproducibility in experiments, as impurities can affect pH and other parameters. Overall, TRIS is a commonly used buffer and valued for its reliability and consistency [45, 46].

2.4 Preparation of human tissues for mechanical testing

The process of the mechanical testing began by immersing the samples in 5% PEG solutions for 24 h. Following this, four dog-bone-shaped samples were taken from each specimen (Figure 6a), two from the attached gingiva and two from the alveolar mucosa. Each at a 90° angle to the other, using a 3D-printed template (Figure 6b) to maintain consistent dimensions

of around 8 mm for testing. Custom clamps made using 3D printing were employed to secure the samples firmly into place (Figure 7) [27]. This comprehensive methodology ensured the systematic acquisition and handling of mucosa samples for the study [40].

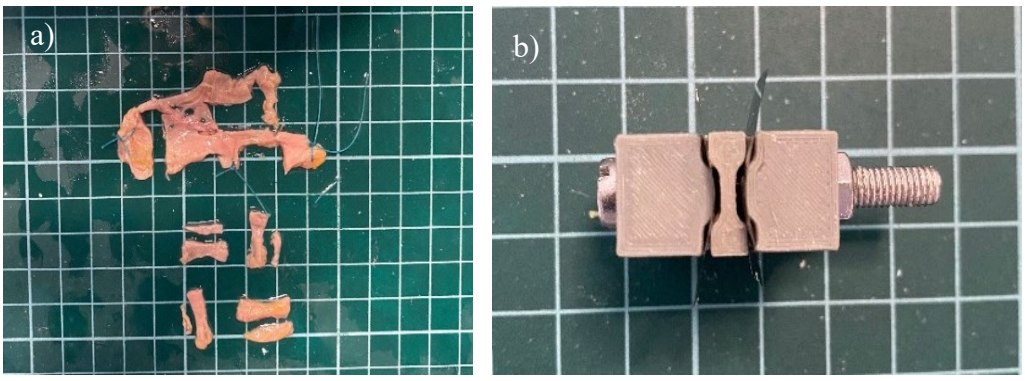

Figure 6: (a) Full Samples shaped into dog-bone for mechanical testing, after 5% PEG submerge, (b) 3D-printed template.

Figure 7: Samples shaped into dog-bone with 3D clamps.

2.5 Scanning

The cross-sectional area was determined using PANASIL, a vinyl polysiloxane, which acted as a mold (Figure 8) and was scanned with the Canon IJ Scan utility in the Fiji ImageJ_win64. This scanning process allowed for precise measurements of the tapered regions dimensions. Before the mechanical tests were conducted, black and white markers (Figure 11) were applied to the samples using standard superglue to ensure accurate tracking of strain during testing. These markers facilitated the observation and analysis of deformation patterns under load [40].

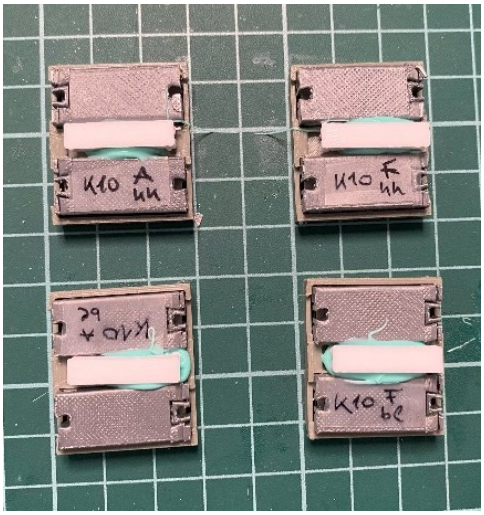

Figure 8: PANASIL use on dog-bone samples to create a mold before mechanical testing.

2.6 Electronical material testing equipment

2.6.1 Autograph Shimadzu

The experiment was conducted using the Autograph Shimadzu AGS-G (Videoextensometer AGS-10kNG, Messphysik ZwickRoell TestingSystems GmbH, Fürstenfeld, Austria), a mechanically built testing rig equipped with a suitable measurement unit, manufactured by a leading company in material testing at the Division of Anatomy at the Medical University of Graz (Figure 9). This multi-column testing machine was designed for universal material testing and is controlled electronically and based on a specific software. The software used for the controlling the test procedure is called WinMTPC (DOLL EDC 60 1278). It can be tailored for specific materials through various adjustable parameters and can produce servo-hydraulic forces over 1000 N. The test samples are secured within a rigid steel frame using two large screw clamps arranged vertically. This configuration allows for the application of vertical force, subjecting the test object to either compression or tension. The machine is capable of measuring various selectable parameters (force, displacement, etc.), which can be defined individually and measured both digitally and optically [47].

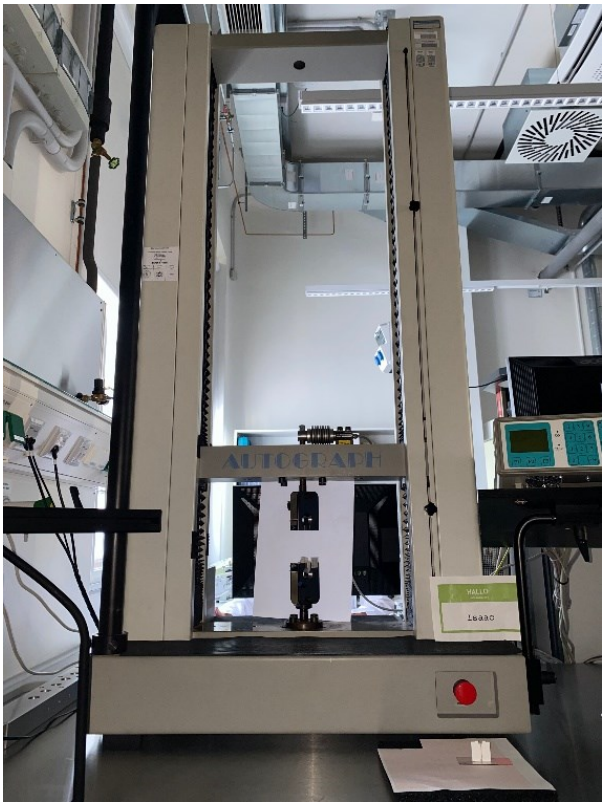

Figure 9: Autograph Shimadzu AGS-G (Videoextensometer AGS-10kNG, Messphysik ZwickRoell TestingSystems GmbH, Fürstenfeld, Austria).

2.6.2 WinextNG

The strain was measured using a video extensometer WinextNG (Videoextensometer ME46 NG, Messphysik Materials Testing GmbH, Fürstenfeld, Austria) (Figure 10) operated with software provided by Messphysik Materials Testing GmbH, Fürstenfeld, Austria. This method allowed for precise, non-contact strain measurement during the tests. The video extensometer provided real-time data, ensuring accurate tracking of deformation throughout the testing process. Additionally, the use of advanced software facilitated efficient data analysis and ensured high reproducibility of the measurements [48].

Figure 10: WinextNG (Videoextensometer ME46 NG, Messphysik Materials Testing GmbH, Fürstenfeld, Austria).

2.7 Preconditioning cycle

To start the procedure, all the prepared dog-bone samples are clamped into the Shimadzu AGS10knG testing machine. Prior to loading until material failure, all samples were subjected to 20 load-unload cycles within a force range of 0.5 N to 2.0 N. Load-displacement readings were conducted at a crosshead displacement rate of 20 mm min^{-1} and a sampling rate of 100 Hz [26, 40].

2.8 Mechanical testing

The stress-deformation behaviour of 44 samples obtained from 11 individuals, 4 samples per individual, (7 females, 4 males) were tested using a Z020 uniaxial testing machine equipped with a 2.5 kN load cell (Xforce P) and test Control II measurement electronics [40].

As explained earlier, randomly distributed black and white markers were placed on the samples. For assessment purposes, a virtual extensometer perpendicular to the surface calculated the nominal strain between two points defined along the samples parallel testing length. Uniaxial tensile tests were conducted at an ambient temperature of 22°C using a universal testing machine [26].

2.9 Uniaxial load-deformation test

Following the preconditioning, the samples were loaded to 2 N and then stretched until failure (Figure 11a-c). Optical deformation data during testing were recorded using a synchronized accurate video tracking of deformation (Videoextensometer ME46 NG, Messphysik Materials Testing GmbH, Fürstenfeld, Austria) [40].

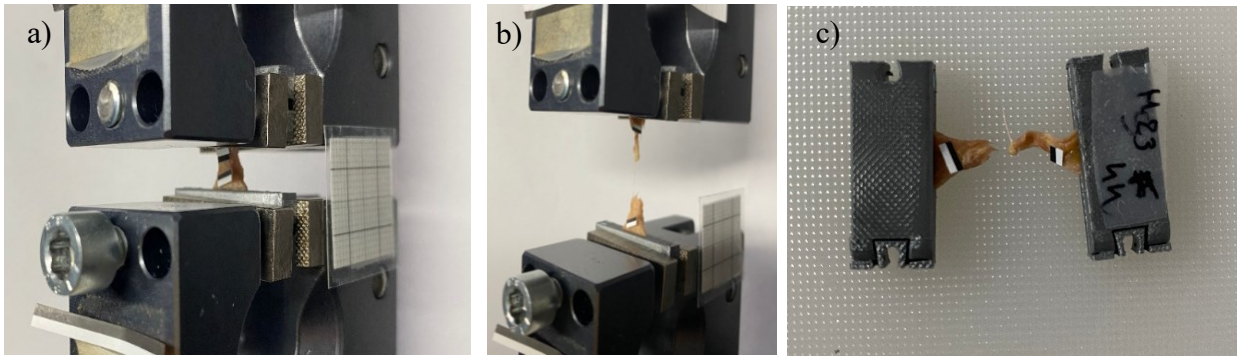

Figure 11: Different dog-bone samples with (a) before mechanical testing with black and white markers, (b) before mechanical testing stretched until failure with black and white markers, (c) after mechanical testing stretched until failure with black and white markers.

2.10 Parameters characterizing material behaviour

2.10.1 Failure stretch

The failure stretch is the maximum strain that a material can withstand before it breaks or fails. It is typically expressed as the ratio of the change in current length (l) to length in reference state (L). It refers to the elongation (lengthening) of a material immediately before it breaks or fails [49]. Failure strain can be calculated as follows:

$$\lambda\,(Failure\ strech) = \frac{l}{L} \tag{3}$$

2.10.2 Failure load

The ultimate load is the force at which a material or structure finally fails and breaks. This can be caused by tension, compression, bending, shear or a combination of these loads. Consequently, the ultimate load is a function of the yield strength of the material and the

number of flaws contained in the test section. The ultimate load is the load that causes the net section stress to equal or exceed the yield strength of the material [50].

2.10.3 Elastic modulus

Young's modulus, also known as modulus of elasticity, is a measure of the hardness of a material. It describes the relationship between stress (force per unit area) and strain (change in length) in a well-behaved material. The modulus of elasticity indicates how much stress is required to achieve strain [51].

The modulus of elasticity E is defined as the ratio of stress (σ) to the resulting strain (ϵ) in the elastic range of the stress-strain curve:

$$E = \frac{\sigma}{\epsilon} \tag{4}$$

2.10.4 Failure Cauchy stress

Cauchy damage stress is the stress that actually occurs in a material where it eventually fails and breaks. These stresses take into account the actual cross-sectional area at the time of damage. This is important because the cross-sectional area decreases during deformation, especially in necking. Necking is a process in which material deforms under stress so that small cracks form in an area just before the material breaks [52].

If F is the force at failure and $A_{Failure}$ is the actual cross-sectional area at failure, then the Cauchy stress at failure σ is defined as:

$$\sigma = \frac{F}{A_{Failure}} \cdot \lambda \tag{5}$$

2.11 Processing of data and statistical analysis

The elastic modulus, failure stretch, and failure Cauchy stress were calculated for all 11 individuals, dependent on their location and orientation of sample retrieval, from the machine data (Videoextensometer ME46 NG, Messphysik Materials Testing GmbH, Fürstenfeld, Austria). Data processing and statistical comparisons were performed using Excel Version 16.15 (Microsoft Corporation, Redmond, WA, USA), MATLAB and Statistics Toolbox Release 2012b (The MathWorks, Inc., Natick, Massachusetts, United States) and GraphPad Prism software version 10 (GraphPad Software, La Jolla, CA, USA) [53].

For the relative water content unpair tests were performed, because of the small sample size ($N<12$ in each group), a nonparametric test would have little or no power to detect a significant difference. Therefore, even though one or two groups did not pass the normality test, we used a parametric test (ANOVA).

2.12 Sample Retrieval for Histology

For future histological examination, small tissue fragments of the intact samples were extracted prior to the material testing, as seen in Figure 6a, and labelled with all relevant data. After the tensile failure tests, the torn samples were also labelled, and the tissue pieces were then shock-frozen at -80°C [27].

3 Results

In the described biomechanical study, both the attached gingiva (n = 22) and the alveolar mucosa (n = 22) were properly applied to all samples (n = 44). All samples that did not reach 2 N in the preconditioning cycle were statistically discarded.

3.1 Osmotic stress adaptation was related to different water content values when compared to the native and the reference condition

If the samples were immersed in a 5 wt% PEG solution for 24 hours, their water content can be recovered close to the original value. The average water content of the native samples in the given control group averaged 64.0 %. The half-life for water removal was calculated to be 8, 12 and 24 hours for PEG concentrations of 2.5 wt%, 5 wt% and 10 wt%, respectively (Figure 12). Following an immersion time of 24 hours, the final mean water content of the samples averaged 78.6%, 65.9% and 78.5% for PEG concentrations of 10 wt%, 5 wt% and 2.5 wt%, respectively. Prolonged immersion in PEG solutions with a concentration of 2.5 wt% led to a decrease in the water content of the mucosa samples, whereas at a PEG concentration of 10 wt% there was an increase. This is unusual, because according to previous studies, there should always be dehydration taking place. Equilibration of the samples in a 5 wt% PEG solution resulted in a water content closest to that of the native samples. A standard exponential equation was used to determine the shortest immersion time required to reach a final water content of 65% in a 5 wt% PEG solution, which corresponds to approximately 24 hours. Consequently, all samples underwent dialysis in a 5 wt% PEG-solution for 24 h prior to material testing [27].

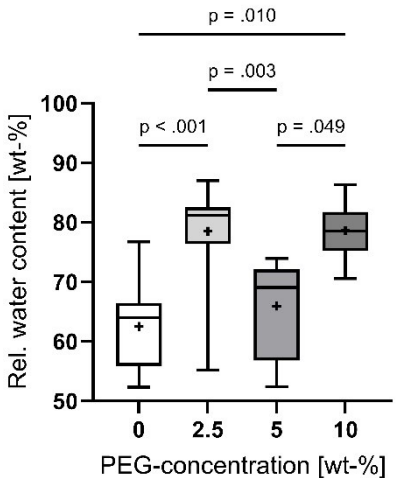

Figure 12: Boxplot of Rel. water content compared to the PEG-concentrations (wt-%).

3.1.1 PEG 2.5%

The effect of immersion in a 2.5% PEG solution on the change in relative water content of human preparations over a 24-hour period (78.53% ± 8.22%) is demonstrated in Table 2 and Figure 13. The graph shows that the change in relative water content peaks after both 8 hours (82.37 ± 7.05%) and 12 hours (80.75 ± 7.81%) of immersion and then declines slightly. This indicates that the preparations are under osmotic stress and are losing water, with the median and mean water content change decreasing over time. The standard deviation shows the dispersion of the data around the average.

Immersion duration (hours)		**0**	**8**	**12**	**24**
Relative water content [%]	Median	63.99	85.13	82.16	81.24
	Mean	62.53	82.37	80.75	78.53
	Standard deviation	7.05	9.40	7.81	8.22

Table 2: Polyethylene glycol - solution of 2.5% - showing median, mean and standard deviation of sample immersion duration in hours.

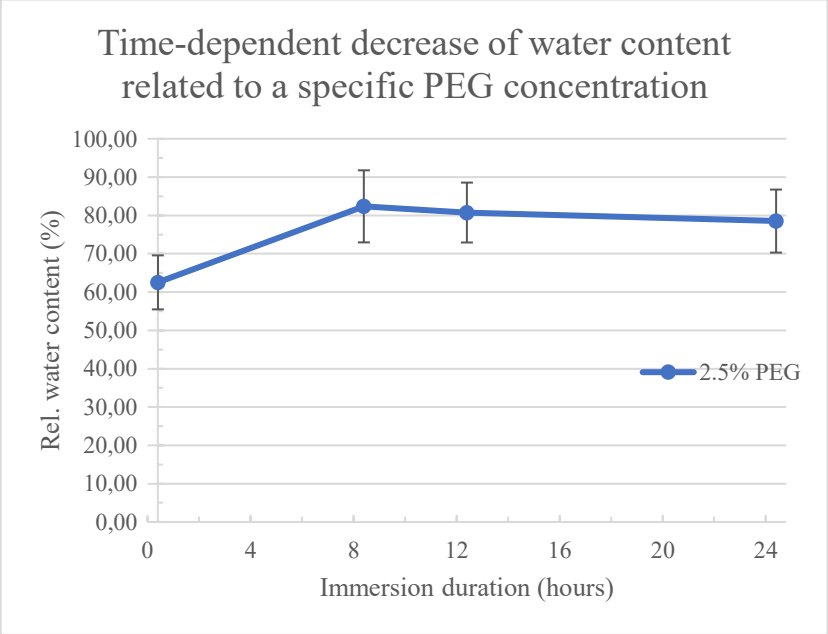

Figure 13: Polyethylene glycol - solution of 2.5% - time-dependent change of water content.

3.1.2 PEG 5%

The effect of immersion in a 5% PEG solution on the change in relative water content of human preparations over a 24-hour period (65.92 ± 7.35%) is displayed in Table 3 and Figure 14. The graph shows, that the change in relative water content varies with time. After 12 hours (83.11 ± 4.40%) of immersion, the median and mean values peak and then decline. This indicates that the samples are under osmotic stress and are losing water, with the standard deviation increasing sharply, particularly after 8 hours (65.37 ± 17.59%) of immersion, indicating a greater dispersion of the data.

Immersion duration (hours)		**0**	**8**	**12**	**24**
Relative water content *[%]*	Median	63.99	71.62	84.94	69.06
	Mean	62.53	65.37	83.11	65.92
	Standard deviation	7.05	17.59	4.40	7.35

Table 3: Polyethylene glycol - solution of 5% - showing median, mean and standard deviation of sample immersion duration in hours.

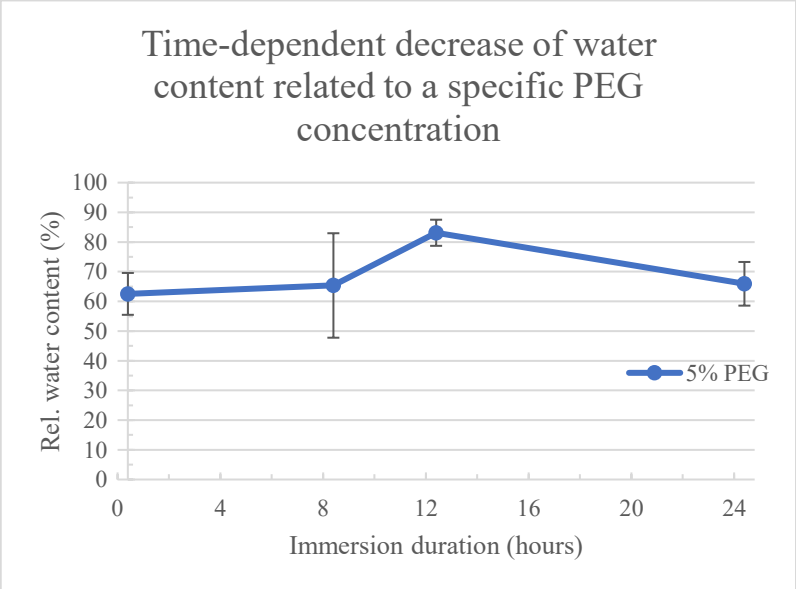

Figure 14: Polyethylene glycol - solution of 5% - time-dependent change of water content.

3.1.3 PEG 10%

The effect of immersion in a 10% PEG solution on the change in relative water content of human preparations over a 24-hour period (78.61 ± 4.23%) is established in Table 4 and Figure 15. The graph shows, that the relative water content change increases with time, with the median and mean increasing up to the 12-hour (76.16 ± 5.76%) mark and then stabilising after 24 hours. The standard deviation shows that the data is becoming less scattered, which could indicate greater consistency in the results. This indicates that the preparations are under osmotic stress and absorb water when immersed in the PEG solution.

Immersion duration (hours)		**0**	**8**	**12**	**24**
Relative water content *[%]*	Median	63.99	76.23	78.55	78.57
	Mean	62.53	74.94	76.16	78.61
	Standard deviation	7.05	9.73	5.76	4.23

Table 4: Polyethylene glycol - solution of 10% - showing median, mean and standard deviation of sample immersion duration in hours.

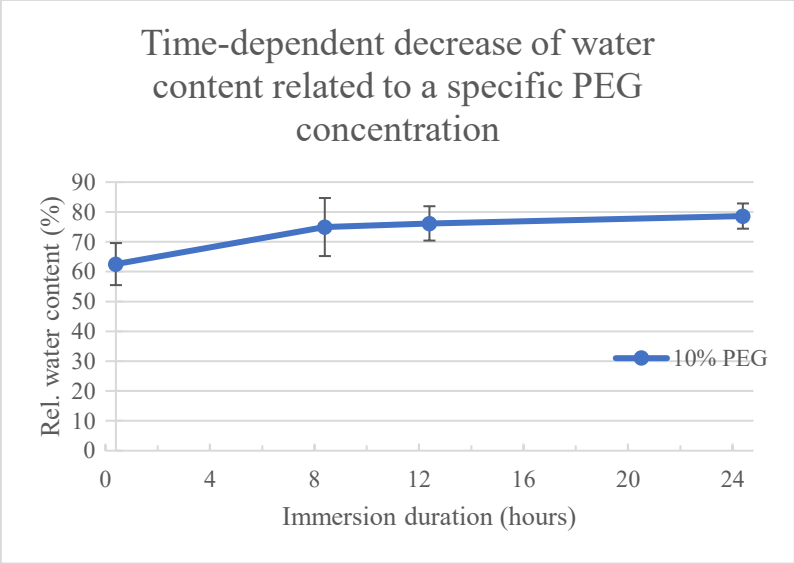

Figure 15: Polyethylene glycol - solution of 10% - time-dependent change of water content.

3.2 Assessment of Tissue Mechanics Tensile properties

3.2.1 Location dependency difference attached to alveolar mucosa

3.2.1.1 Stretch at failure

The stretch at failure load of the tissue samples showed location-dependent differences, ranging from 1.649 ± 0.25 N in the attached gingiva region to 1.643 ± 0.23 N in the alveolar mucosa region (Table 5 and Figure 16a). A statistically not significant difference was observed between the attached gingiva and alveolar mucosa groups ($p = 0.77$).

3.2.1.2 Failure Cauchy stress

The failure Cauchy stress versus stretch plots for the samples of the two groups are depicted in Figure 16b. It revealed significant statistical p value of 0.001 as well as a correlation with the failure stretches shown in Figure 17 a-d. Furthermore, it was found that the attached gingiva group 4.2 ± 3.7 MPa had a higher failure Cauchy stress level compared to the alveolar gingiva 1.5 ± 1.3 MPa.

3.2.1.3 Failure load

The failure load of the tissue samples in location dependent differences ranged from 9.4 ± 9.3 N in the region of the attached gingiva to the alveolar mucosa with 5.4 ± 6.4 N (Table 5 and Figure 16c), with a statistical significance observed between attached gingiva and alveolar mucosa group ($p = 0.013$). This suggests that the attached gingiva can withstand higher loads compared to the alveolar mucosa.

3.2.1.4 Elastic modulus

The highest mean elastic modulus of 19.4 ± 17.5 MPa was found in the attached gingiva group, followed by the samples from the alveolar mucosa (4.8 ± 3.3 MPa) as shown in Table 5 and Figure 16d. The elastic moduli of attached gingiva was statistically different to the buccal mucosa ($p = 0.003$). However, four samples of the attached gingiva and three samples of the alveolar gingiva did not meet the maximum 2 N in preconditioning and where therefore not statistically relevant and excluded.

	Stretch at failure (-)	Failure Cauchy stress (MPa)	Failure load (N)	Elastic modulus (MPa)
Attached gingiva	1.649 ± 0.25	4.2 ± 3.7	9.4 ± 9.3	19.4 ± 17.5
Alveolar mucosa	1.643 ± 0.23	1.5 ± 1.3	5.4 ± 6.4	4.8 ± 3.3

Table 5: Showing mean ± standard deviation of location dependency mechanical testing results of attached gingiva vs. alveolar mucosa.

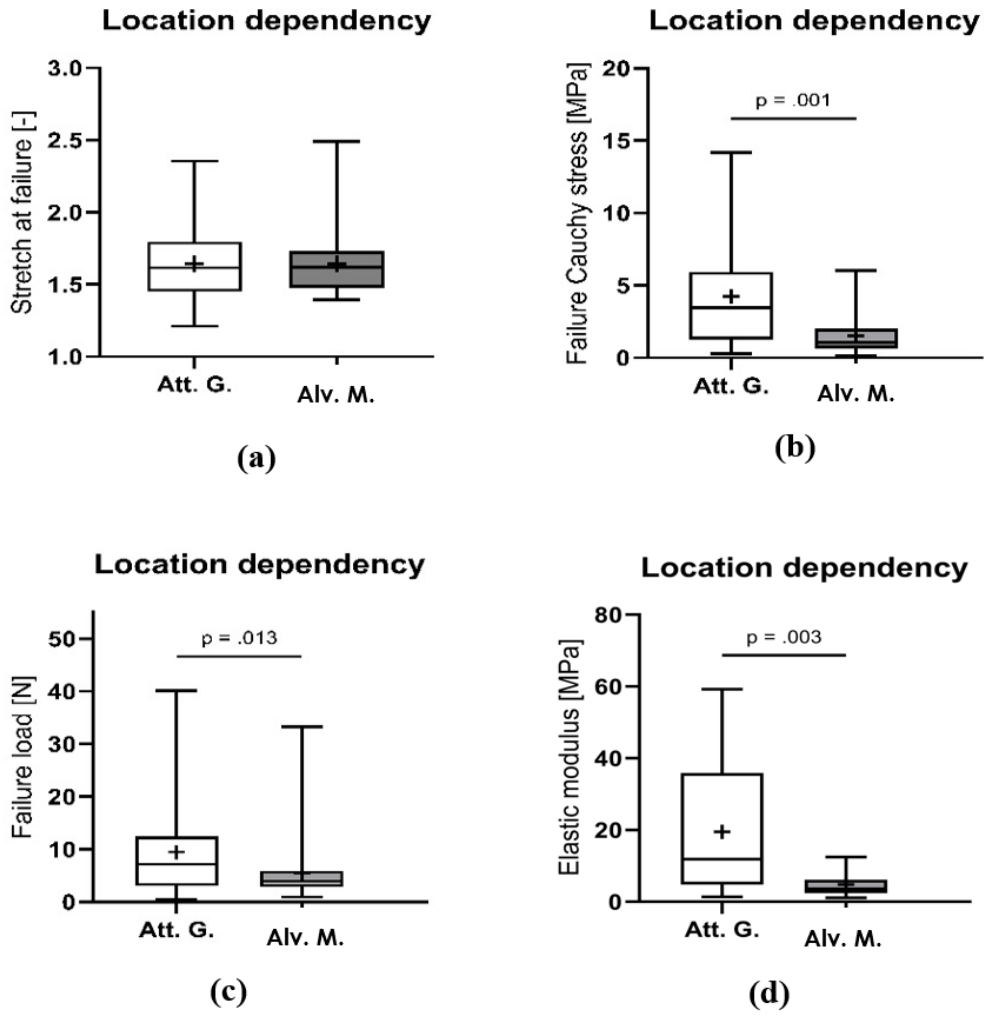

Figure 16: Graphs showing location dependency of attached gingiva (Att. G.) vs. alveolar mucosa (Alv. M.) (a) Stretch at failure (b) Failure Cauchy stress, (c) Failure load and (d) elastic modulus.

3.2.2 Direction dependency of mandible crest and bucco-lingual directions

3.2.2.1 Stretch at failure

The direction-dependent stretch at failure of the tissue samples varied in the attached gingiva region from 1.7 ± 0.2 N in the bucco-lingual direction to 1.5 ± 0.1 N at the mandibular crest (Table 6 and Figure 20a). In addition, a similar stretch at failure was observed in the alveolar mucosa region, ranging from 1.6 ± 0.1 N in the bucco-lingual direction to 1.6 ± 0.2 N at the mandibular crest. There was no statistically significant difference between the bucco-lingual and mandibular crest directions in the attached gingiva ($p = 0.27$) or in the alveolar mucosa sections ($p = 0.89$).

3.2.2.2 Failure Cauchy stress

Cauchy stress vs. strain plots for samples of both groups attached gingiva and alveolar mucosa are shown in Figure 20b. Looking at the location, there is a statistical difference between these two groups ($p = 0.001$). However, as indicated in Table 6, there was no significant correlation in failure stress between the mandibular crest (4.9 ± 3.1 MPa) group and the bucco-lingual (3.4 ± 4.07 MPa) group in both the attached gingiva ($p = 0.3665$) and between the mandibular crest (1.3 ± 0.8 MPa) group and the bucco-lingual (1.64 ± 1.63 MPa) group alveolar mucosa ($p = 0.765$). This indicates that the directional differences in stress response are not statistically significant in these tissue types.

The representative stress-strain curves (Figure 17 a-d) showed typical behaviour of soft connective tissues, featuring an initial toe region followed by a gradual increase in tensile force until tissue failure. These stresses take the actual cross-sectional area at the time of damage into account. This is important, because the cross-sectional area decreases during deformation.

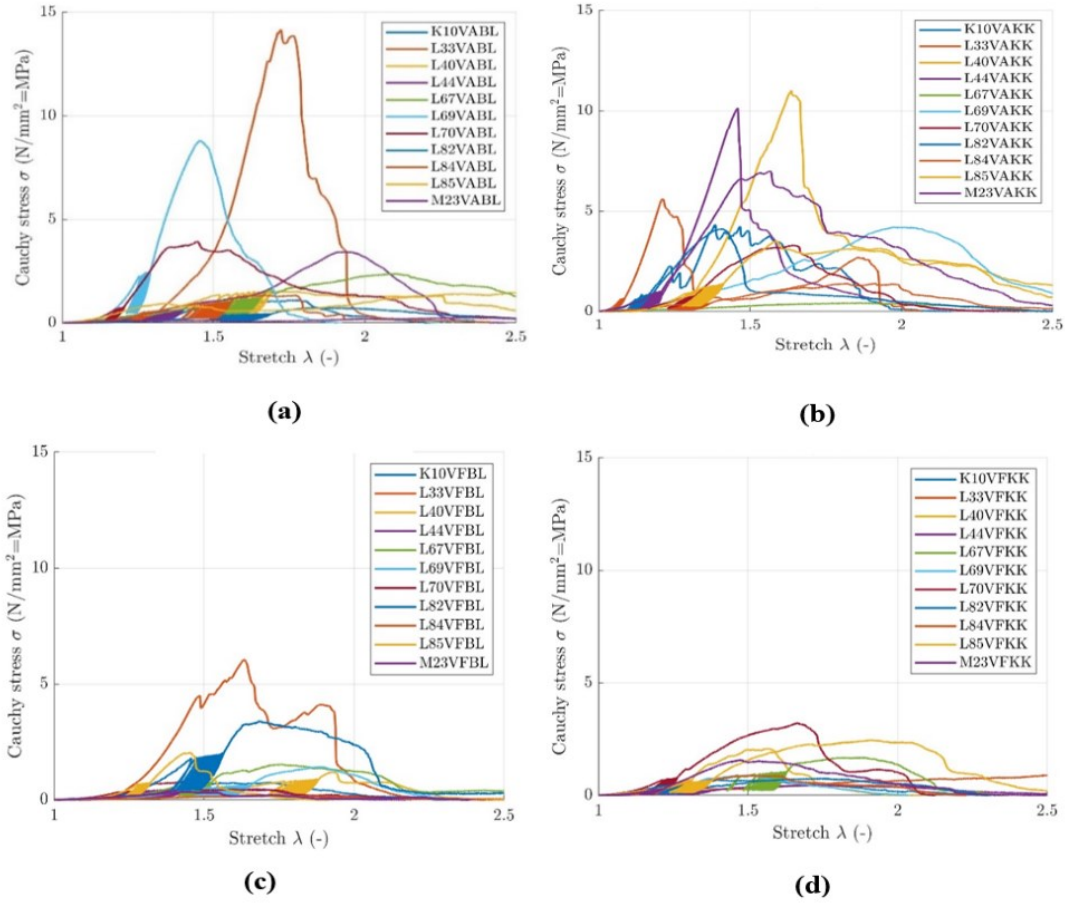

Figure 17: Cauchy stress stretch plots for all samples in the attached gingiva and alveolar mucosa region with mandible crest and bucco-lingual directions: attached gingiva (a) bucco-lingual and (b) mandible crest, alveolar mucosa (c) bucco-lingual and (d) mandible crest group. The ID of every sample is displayed in the right-hand corner of each graphic. The failure Cauchy stress is the true stress in the material at the time of failure and takes into account the reduced cross-sectional area due to deformation and necking.

3.2.2.2.1 Cross section area

In a location and direction dependent manner, the alveolar mucosa demonstrated the biggest cross sectional area. The cross section of 6.5 ± 3.2 mm^2 in the alveolar gingiva region, is significantly greater than the attached mucosa's 3.9 ± 1.8 mm^2 (p = 0.001) (Figure 18a). However, there was no significant directional difference in cross sections between the bucco-lingual 4.2 ± 2.2 mm^2 and mandibular crest 3.6 ± 1.3 mm^2 aspects of the attached gingiva (p = 0.49) or between the bucco-lingual 6.0 ± 2.3 mm^2 and mandibular crest 7.0 ± 3.8 mm^2 sections of the alveolar mucosa (p = 0.36) (Table 18b).

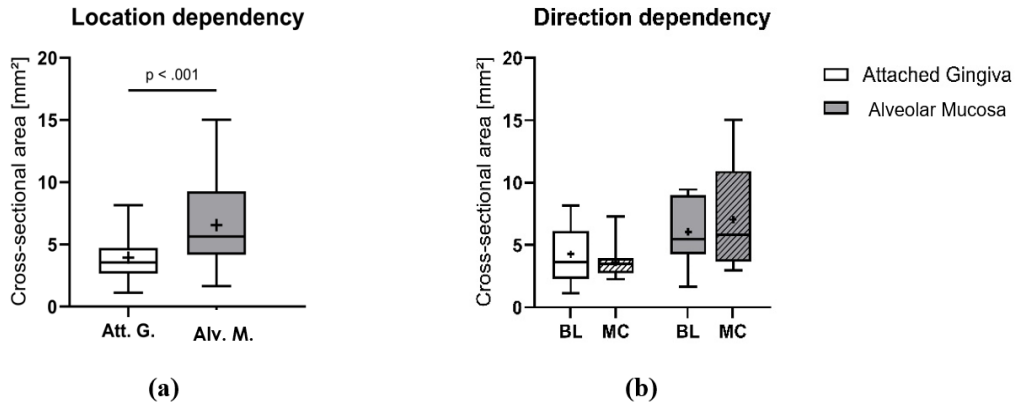

Figure 18: Graphs showing cross section of (a) attached gingiva (Att. G.) vs. alveolar mucosa (Alv. M.) plots for all samples and (b) the attached gingiva and alveolar mucosa region with mandible crest (MC) and bucco-lingual (BL) directions.

3.2.2.3 Failure load

The failure load of the tissue samples with direction dependency ranged in the attached gingiva region from bucco-lingual 7.6 ± 10.6 N to mandible crest 11.3 ± 7.3 N (Table 6 and Figure 20c). Furthermore, in the alveolar mucosa region a lower failure load was detected between bucco-lingual 5.9 ± 8.7 N and mandible crest 4.9 ± 2.3 N. No statistical significance was observed between the bucco-lingual and mandible crest direction of the attached gingiva ($p = 0.14$) or between the bucco-lingual and mandible crest of the alveolar mucosa sections ($p = 0.32$).

3.2.2.4 Elastic modulus

The attached gingiva demonstrated in location dependency the highest tensile stiffness with a Young's modulus of 18 ± 21 MPa, significantly greater than that of the alveolar mucosa (6.1 ± 4.1 MPa). However, direction dependent there was no significant difference in stiffness between the bucco-lingual (17.7 ± 19.9 MPa) and mandibular crest (20.8 ± 15.1 MPa) aspects of the attached gingiva ($p = 0.36$), or between the bucco-lingual (6.11 ± 3.8 MPa) and mandible crest (3.5 ± 2.1 MPa) of the alveolar mucosa sections ($p = 0.133$) (Table 6 and Figure 20d). The elastic range is the range in which the material behaves linearly and returns to its original shape after being relieved. The plastic range lies beyond the yield point, where the material begins to deform plastically, therefore a

permanent deformation remains after the load is removed. In this area, the curve is no longer linear, depicted in Figure 19.

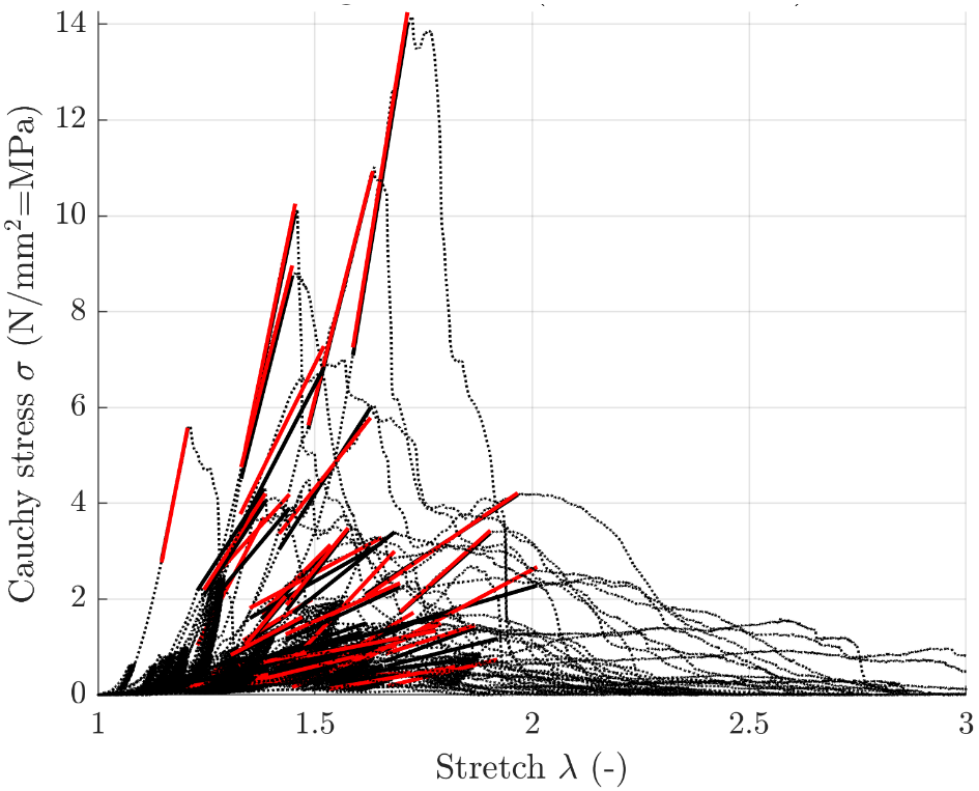

Figure 19: Showing all graphs of attached gingiva and alveolar mucosa of the elastic modulus mechanical testing results.

		Stretch at failure (-)	Failure Cauchy stress (MPa)	Failure load (N)	Elastic modulus (MPa)
Attached gingiva	BL	1.7 ± 0.2	3.4 ± 4.07	7.6 ± 10.6	17.7 ± 19.9
	MC	1.5 ± 0.1	4.9 ± 3.1	11.3 ± 7.3	20.8 ± 15.1
Alveolar mucosa	BL	1.6 ± 0.1	1.64 ± 1.63	5.9 ± 8.7	6.11 ± 3.8
	MC	1.6 ± 0.2	1.3 ± 0.8	4.9 ± 2.3	3.5 ± 2.1

Table 6: Showing mean ± standard deviation of direction dependency mechanical testing results of attached gingiva vs. alveolar mucosa for all samples in the attached gingiva and alveolar mucosa region with mandible crest (MC) and bucco-lingual (BL) directions.

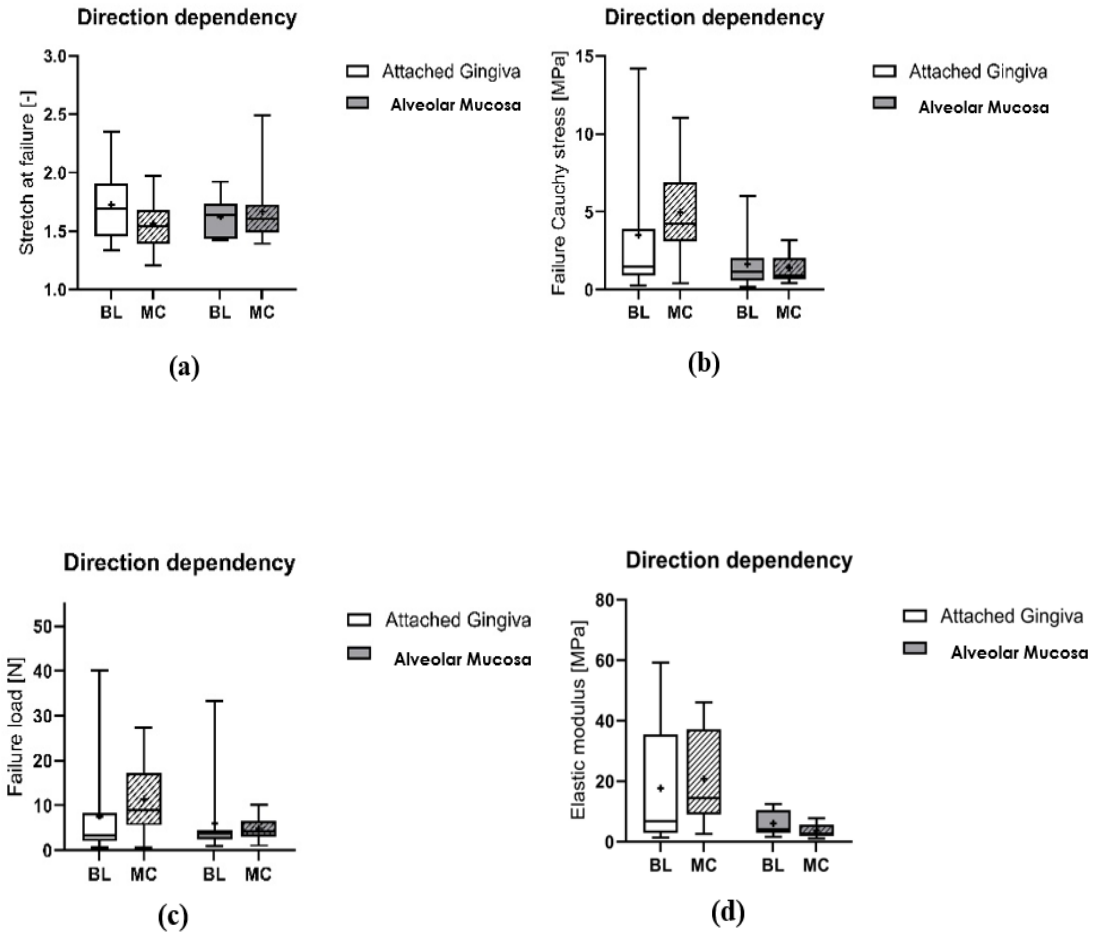

Figure 20: Graphs showing direction dependency of attached gingiva vs. alveolar mucosa plots for all samples in the attached gingiva and alveolar mucosa region with mandible crest (MC) and bucco-lingual (BL) directions: (a) stretch at failure (b) failure Cauchy stress, (c) failure load and (d) elastic modulus.

4 Discussion

This study is the first to demonstrate the feasibility of using unembalmed tissues to study human oral mucosa, allowing direct comparison between tissues from two intraoral regions. The null hypothesis, which posited a difference in elastic modulus and tensile properties of oral mucosal tissues from various intraoral locations, was confirmed. The results indicate, that mucosal tissues from different intraoral regions exhibit different mechanical behaviours. Furthermore, it suggests, that regional variations in tissue structure significantly influence their mechanical properties. Future research should investigate the underlying biological factors that contribute to these differences to improve our understanding of oral tissue biomechanics.

4.1 Osmotic stress protocol

Adjusting the water content of soft tissues is crucial to minimize unpredictable effects on their biomechanics and to ensure reliable results that accurately represent their state in living conditions. The water content is a critical factor in soft tissue biomechanics [40]. Therefore, the aim of the osmotic stress protocol was to adjust to the water content of tissues prior to biomechanical testing.

To alter the water content of human samples the osmotic stress protocol was employed, allowing us to assess mechanical properties in a standardized manner. The duration of submersion can affect the water content. In this study, a consistent submersion time of 24 hours in a 5% PEG solution was used, guided by the control group results. PEG, as an osmotically active agent, has proven effective in mechanical applications.

A previous study [54] showed, that after storage of cortical bone in saline solution for different durations (3, 10, 36, and 60 days), the tissue elastic modulus and ultimate strength decreased, likely because the organic matrix, mainly collagen, deteriorated over time. To ensure consistent results, all the samples were collected from the same anatomical site on body doners, loaded uniaxially, and tested using custom 3D-printed clamps developed in our lab to minimize material slippage.

The results of the OSP in this study presented, showed inconclusive results in the four groups of 0, 8, 12 and 24 hours in their different PEG groups. Closest to the control group was the group immersed in 5% PEG solution for 24 hours. However, the 2.5% and 10% groups did not show the dehydration previously suggested by various studies [27, 40]. One possible reason for this issue might be the freshness of the body donors. Completely unembalmed specimens, when stored in a cool refrigerator environment, remain in good condition for only a few days before deteriorating quickly. While unembalmed specimens frozen at -80°C for later use, the texture may be damaged and the specimens will only be preserved as long as they remain frozen [17]. Another reason could be the long cooling period at -80°C degrees, where a break in the cooling chain cannot be ruled out. This could lead to the assumption that the cell structure was damaged and the cells no longer had the opportunity to maintain osmosis during the OSP.

A further study may be examine the samples histologically to determine the cause of these results. The question is whether the cooling process was too long and the cells were damaged, which could affect the OSP. In addition, it will be important to determine whether the cooling rate affected the structural integrity of the tissues, potentially leading to altered mechanical properties. Another factor to be investigated is whether changes in the extracellular matrix composition occurred during the cooling process, which could affect the overall biomechanical behaviour. Understanding these aspects will help to clarify the underlying reasons for the observed differences and improve future tissue preservation techniques.

4.2 Mechanical testing

4.2.1 Direction and location dependency

As shown in the Results section, there are statistically proved differences in the location-dependent region, but none in the direction-dependent region. This means, that the biomechanical properties vary depending on the position within the tested area, but remain constant regardless of the direction of the cell structure. This finding emphasizes the importance of accurate sample retrieval and placement in biomechanical testing to ensure valid and reproducible results. Additionally, it suggests, that specific regions within the tissue may be inherently stronger or weaker, potentially impacting clinical outcomes.

Understanding these regional variations can aid in the development of targeted treatments and interventions. Furthermore, this insight can improve the design of biomaterials and prosthetics, that better mimic the natural behaviour of oral tissues.

4.2.1.1 Significant biomechanical location-dependent differences between attached gingiva and alveolar mucosa

Looking at the results of the location-dependent section, one can observe, that there are statistically significant differences in the categories of Young's modulus ($p = 0.003$), Cauchy stress ($p = 0.001$), and failure load ($p = 0.013$). It can also be seen, that the attached gingiva has the highest values in each of these categories, compared to the alveolar mucosa. This suggests that the attached gingiva is mechanically stronger and more resilient under load, than the alveolar mucosa. The higher Young's modulus values indicate greater stiffness, while the higher Cauchy stress and ultimate load values indicate a greater ability to resist deformation and failure. These differences highlight the importance of considering tissue type and location when evaluating biomechanical properties in dental research and clinical applications.

4.2.1.2 Consistent mechanical properties of oral tissues with direction dependent samples

The results of the direction-dependent samples showed no significant statistical difference between the mandibular crest and bucco-lingual directions in any section of the alveolar gingiva and attached mucosa. There was no statistical difference between the mandibular crest and the bucco-lingual direction for the four test points: Young's modulus, ultimate Cauchy stress, ultimate strain, and ultimate load. This indicates, that the mechanical properties of these tissues are consistent regardless of the direction of the cell structure. This consistency suggests that the structural composition of the alveolar gingiva and attached mucosa may be isotropic in nature. These findings provide a better understanding of the mechanical behaviour of oral tissues and can revolutionize clinical practice and material design in dentistry.

4.2.2 Thiel embalming impact on mechanical properties

A previous study [1] has tested biomechanical properties using Thiel-fixed mucosal samples and the results were similar to those of the samples tested in this study. In terms of E-module, the Thiel embalmed attached gingiva group exhibited the highest elastic modulus at 37.36 ± 17.4 MPa, with lower values found in the hard palate and buccal mucosa groups. The difference in elastic modulus between the attached gingiva and buccal mucosa was statistically significant ($p = 0.01$).

The sample results of this study were 19.4 ± 17.5 MPa for the E-modulus of elasticity in the attached mucosa and 4.8 ± 3.3 MPa in the alveolar mucosa ($p = 0.003$). The common feature of these studies relates to the preparation of the samples using OSP and similar test procedures. The difference between these two studies is obviously the type of fixation with Thiel solution of the samples and the number of body donors. In a previous study [1] a body donation number of two was used, but they subsequently used a similar sample number to the study presented. Both studies showed a higher value of elastic module in the region of the attached gingiva and a lower value in the region of the alveolar mucosa.

The present study addresses the biomechanical properties of unfixed specimens. The preferred method for biomechanical testing of human soft tissue is to store the tissue in a fresh-frozen state. This approach separates the tissue procurement process, which typically must be completed shortly after the body donor's death, from the material testing phase [55]. However, only few studies provide information on storage protocol or tissue changes and, at -80°C, biomechanical properties over time. Therefore, it is unclear how long storage, in this case several months, affects the biomechanical properties of these specimens. This gap in knowledge highlights the need for further research to determine the optimal storage conditions and duration for maintaining tissue integrity. Understanding these factors is crucial for ensuring the reliability and accuracy of biomechanical testing in future studies.

Nevertheless, there is limited research on how Thiel embalming affects tissue properties in both human and animal tissues. Some studies suggest, that Thiel embalming may alter the mechanical properties of human soft tissues. The evidence indicates, that Thiel-embalmed

tissues might not accurately reflect lifelike biomechanical behaviour under quasi-static conditions, and this inconsistency could also apply to conditions with much higher loading rates, due to the viscoelastic nature of extracellular matrix tissues [1].

Following this study, the tested samples will be examined histologically, which will provide further insight into why there is a higher Young's modulus in the attached gingiva than in the alveolar mucosa. One can suggest different compositions of the two different oral sites. The adherent mucosa is composed of a multi-layered, highly keratinised squamous epithelium, which is expected to have a higher modulus of elasticity, than the weakly keratinised, multi-layered squamous epithelium of the alveolar mucosa.

4.2.3 Importance of sample quantity

Although limited by the number of human specimens available and the variability between samples, the intact oral mucosa used in the present study demonstrated the potential for better characterization of mechanical properties to better refine future simulations and calculations. Although the differences in physical properties among the 11 body donors were not statistically significant, future studies should stratify donor age, gender, and health status to minimize differences. Follow-up studies and histological evaluations to failure and tissue sampling are also needed. Fresh, unembalmed tissue is also the gold standard because in both human and animal tissue, there is limited research on how Thiel embalming affects tissue properties [25, 56].

Therefore, future studies with larger numbers of samples from multiple body donors would be useful in investigating the relationship between mechanical properties and mucosal volume as well as the relationship between mucosa and attached gingiva [38].

4.3 Optimization of biomechanical models by analysing the tensile strength and histological examination of unembalmed tissue

In a further study, the samples tested, that were subjected to the Ultimate Tensile Strength test (UTS) will be histologically examined. This will provide further information and insight

into the values tested here and the significance of testing on fresh tissue as opposed to fixed tissue. By analysing the tear resistance and histological structure, we aim to better understand the mechanical integrity and microstructural changes resulting from unembalmed tissue samples. This additional data will help clarify the extent to which for example Thiel embalming affects tissue behaviour and provide insight into optimizing testing protocols for both fresh and preserved tissues. Ultimately, this study will contribute to more accurate biomechanical models and improved methods for evaluating tissue properties.

5 Conclusion and Future Perspectives

The findings of this study indicate, that tissues from different intraoral regions exhibit distinct morphological and mechanical behaviours, which may be confirmed in the future by histological analysis.

Employing the osmotic stress technique to regulate the water content of tissues is strongly recommended as an essential aspect of biomechanical testing. This approach ensures, that the mechanical properties of the tissues are maintained in a state, that closely mimics their natural condition. Further research is necessary to fully comprehend the impact of water content on other mechanical properties, such as tensile strength, failure stretch and elastic modulus. Additionally, understanding how water content effects the microstructural integrity of tissues will be crucial in developing more accurate and reliable biomechanical models.

Overall, there is insufficient evidence describing regional biomechanical variations and the relationship between different mechanical zones and tissue structure. However, more studies are needed to map these variations comprehensively and to correlate them with specific structural characteristics within the tissues. The biomechanical response of the oral mucosa to occlusal loads is also not well understood. Investigating how different regions of the oral mucosa respond to different levels and types of loading will provide valuable insights into their functional roles and potential vulnerabilities. Moreover, eliminating these responses will aid in the development of better dental materials and treatment strategies that can accommodate or mitigate biomechanical stresses.

6 References

1. Choi, J.J.E., et al., *Mechanical properties of human oral mucosa tissues are site dependent: A combined biomechanical, histological and ultrastructural approach.* Clin Exp Dent Res, 2020. **6**(6): p. 602-611.
2. Waschke, F.P.P.P.J., *Sobotta Atlas der Anatomie für Zahnmedizin*. 2023: Urban & Fischer in Elsevier.
3. Anderhuber, F., F. Pera, and J. Streicher, *Waldeyer - Anatomie des Menschen*. 2012: Walter de Gruyter.
4. Dauber, W., H. Feneis, and H. Feneis, *Pocket atlas of human anatomy : founded by Heinz Feneis*. 5th rev. ed. 2007, Stuttgart ; New York: Thieme. 545 p.
5. Michael Schünke, E.S., Udo Schumacher, *PROMETHEUS Kopf, Hals und Neuroanatomie*. Vol. 6. 2022: Thieme. 616.
6. Platzer, W., *1Bewegungsapparat*. Vol. 12. 2018: Thieme.
7. Whetzel, T.P. and C.J. Saunders, *Arterial anatomy of the oral cavity: an analysis of vascular territories.* Plast Reconstr Surg, 1997. **100**(3): p. 582-7; discussion 588-90.
8. Brizuela M, W.R., *Histology, Oral Mucosa.* StatPearls Publishing, 2023.
9. Edmans, J.C., Katharina & Murdoch, Craig & Hatton, Paul & Spain, Sebastian & Colley, Helen *Mucoadhesive Electrospun Fibre-Based Technologies for Oral Medicine* Pharmaceutics, 2020.
10. Renate Lüllmann-Rauch, E.A., *Taschenlehrbuch Histologie*. Vol. 6. 2019: Thieme.
11. Klokkevold, P., *Carranza's Clinical Periodontology*. Vol. 12. 2015: Elsevier.
12. Kydd, W.L. and C.H. Daly, *The biologic and mechanical effects of stress on oral mucosa.* J Prosthet Dent, 1982. **47**(3): p. 317-29.
13. Gaballah, K.Y. and I. Rahimi, *Can presence of oral Fordyce's granules serve as a marker for hyperlipidemia?* Dent Res J (Isfahan), 2014. **11**(5): p. 553-8.
14. Wolf, H.F., *Periodontology*. 3rd rev. and expanded ed. Color atlas of dental medicine. 2005, Stuttgart ; New York: Thieme ;. xi, 532 p.
15. SL, O., *Attached gingiva: Histology and surgical augmentation.* 2009.
16. Navya, P.D. and A. Rajasekar, *Management of inadequate width of attached gingiva using mucograft.* J Adv Pharm Technol Res, 2022. **13**(Suppl 1): p. S358-S361.
17. Anderson, S.D., *Practical light embalming technique for use in the surgical fresh tissue dissection laboratory.* Clin Anat, 2006. **19**(1): p. 8-11.
18. Kydd, W.L., Mandley, J., *Stiffness of palatal mucoperiosteum.* The Journal of Prosthetic Dentistry, 1967. **18**: p. 116-121.
19. Picton, D.C. and D.J. Wills, *Viscoelastic properties of the periodontal ligament and mucous membrane.* J Prosthet Dent, 1978. **40**(3): p. 263-72.
20. Thiel, W., *[The preservation of the whole corpse with natural color].* Ann Anat, 1992. **174**(3): p. 185-95.
21. Thiel, W., *[Supplement to the conservation of an entire cadaver according to W. Thiel].* Ann Anat, 2002. **184**(3): p. 267-9.
22. G, A., S. Ray, and S. Mohapatra, *Preparation of Soft Embalmed Cadavers by the Modified Thiel Embalming Technique for Surgical Skill Training and Development of a Universal Quantitative Scoring System to Assess the Suitability of Soft Embalmed Cadavers for Such Training Purposes.* Cureus, 2023. **15**(8): p. e43991.

23. Liao PY, W.Z., *Thiel-embalming technique: investigation of possible modification in embalming tissue as evaluation model for radiofrequency ablation.* J Biomed Res., 2019. **4**.
24. Hammer, N., *Thirty years of Thiel embalming-A systematic review on its utility in medical research.* Clin Anat, 2022. **35**(7): p. 987-997.
25. Hammer, N., et al., *Comparison of modified Thiel embalming and ethanol-glycerin fixation in an anatomy environment: Potentials and limitations of two complementary techniques.* Anat Sci Educ, 2015. **8**(1): p. 74-85.
26. Zwirner, J., et al., *Tissue biomechanics of the human head are altered by Thiel embalming, restricting its use for biomechanical validation.* Clin Anat, 2019. **32**(7): p. 903-913.
27. Hammer, N., *Do Cells Contribute to Tendon and LigamentBiomechanics?* PLOS ONE, 2014. **9**.
28. Schleifenbaum, S., et al., *Tensile properties of the hip joint ligaments are largely variable and age-dependent - An in-vitro analysis in an age range of 14-93 years.* J Biomech, 2016. **49**(14): p. 3437-3443.
29. Gologan D., S.A.E., Stsn R, *Factors influenzing the quality of formaldehyde fixed paraffin embedded tissue samples- review.* Rev. Rom. Med. Vet, 2021. **31(4),** : p. 87-92.
30. Subasi, N.T., *Formaldehyde Advantages and Disadvantages: Usage Areas and Harmful Effects on Human Beings.* Biochemical Toxicology - Heavy Metals and Nanomaterials, 2020.
31. Fox, C.H., et al., *Formaldehyde fixation.* J Histochem Cytochem, 1985. **33**(8): p. 845-53.
32. Wilke, H.J., S. Krischak, and L.E. Claes, *Formalin fixation strongly influences biomechanical properties of the spine.* J Biomech, 1996. **29**(12): p. 1629-31.
33. *https://gestis.dguv.de/data?name=010520,* , in *GESTIS-Stoffdatenbank*. Accessed: 19.Jun.2024.
34. N.T., S., , in *Biochemical Toxicology: Heavy Metals and Nanomaterials*, I.O.K. Ince M., Ondrasek G, Editor. 2020, IntechOpen. p. 101-107.
35. Solt P., K.J., Gindl-Altmutter W., Kantner W., Moser J., Mitter R.d, Herwijnen H. W.G.,, *Technological performance of formaldehyde-free adhesive alternatives for particleboard industry.* International Journal of Adhesion and Adhesives, 2019. **94**: p. 99-131.
36. Duong A., S.C., McHale C. M., Vaughan C. P., Zhang L.,, *Reproductive and development toxicity of formaldehyde: A systematic review.* Mutat. Res., , 2011. **728**(3): p. 118-38.
37. Chen, J., et al., *Biomechanics of oral mucosa.* J R Soc Interface, 2015. **12**(109): p. 20150325.
38. Goktas, S., J.J. Dmytryk, and P.S. McFetridge, *Biomechanical behavior of oral soft tissues.* J Periodontol, 2011. **82**(8): p. 1178-86.
39. Lacoste-Ferre, M.H., Demont, P., Dandurand, J., Dantras, E., Duran, D., & Lacabanne, C. , *Dynamic mechanical properties of oral mucosa: Comparsion with polymeric soft denture liners.* Journal of the Mechanical Behavior of Biomedical Materials, 2011. **4**: p. 269-274.
40. Lozano, P.F., et al., *Water-content related alterations in macro and micro scale tendon biomechanics.* Sci Rep, 2019. **9**(1): p. 7887.
41. *SPECTRUM PRODUCT INSTRUCTION MANUAL*. 2022, Spectrum Laboratories Inc.

42. *Der Missing Link-Eppendorf Tubes® 5.0 mL – einfach und sicher mit System*, E.A.G.W. Austria, Editor., Eppendorf AG.
43. *Quintix® and Secura®Standard Laboratory Balances: Reliable Weighing for Faster and Better Results*. 2022, Sartorius Lab Instruments GmbH & Co. KG
44. Hagel, V., T. Haraszti, and H. Boehm, *Diffusion and interaction in PEG-DA hydrogels.* Biointerphases, 2013. **8**(1): p. 36.
45. Y.A. Kondratenko, A.A.N., A.A. Zolotarev, M.Y. Arsent'ev, G.G. Nyanikova, V.L. Ugolkov, E.I. Sysoev, T.A. Kochina, *Synthesis, structure and properties of tris(hydroxymethyl)aminomethane complexes with biogenic metal salts.* Inorganica Chimica Acta, 2022. **530**.
46. *https://gestis.dguv.de/data?name=100571*. Accessed : 23.06.2024, GESTIS-Stoffdatenbank.
47. Wallner, D.m.u.J., *Die Anwendung der Herbert-Knochen-Schraube in der osteosynthetischen Behandlung von Frakturen des Kieferwinkels: Ein biomechanischer Vergleich zur konventionellen Miniplattenosteosynthese* in *Doktor der medizinischen Wissenschaften (Dr.scient.med.)*. 2015: Medizinischen Universität Graz, Mund-, Kiefer- und Gesichtschirurgie
48. Grosser, P., Siegel, C., Neinhuis, C., and Lautenschlaeger, T, *Triumfetta cordifolia: A Valuable (African) Source for Biocomposites.* 2018. **13(4)**: p. 7671-7682.
49. Shirsha Bose, S.L., Elisa Mele, Vadim V. Silberschmidt, *Fracture Behaviour of Collagen: Effect of Environment.* Procedia Structural Integrity, 2020. **28**: p. 843-849.
50. F. Laurin, N.C., J.-F. Maire, *19 - Strength prediction methods for composite structures: Ensuring aeronautical design office requirements*, in *Numerical Modelling of Failure in Advanced Composite Materials*, S.R.H. Pedro P. Camanho, Editor. 2015, Woodhead Publishing. p. 507-532.
51. David R.H. Jones, M.F.A., *Chapter 3 - Elastic Moduli*, in *Engineering Materials 1- An Introduction to Properties, Applications and Design*. 2019. p. 31-47.
52. Stéphane Avril, M.B., Michel Cosson, Poul Nielsen,, *Chapter 5 - Inverse problems in the characterization of soft connective tissue: perspective for reproduction system*, in *In Biomechanics of Living Organs,Biomechanics of the Female Reproductive System: Breast and Pelvic Organs,*. 2023. p. 115-138.
53. Zwirner, J., et al., *Tensile properties of the human iliotibial tract depend on height and weight.* Med Eng Phys, 2019. **69**: p. 85-91.
54. Guanjun Zhang, X.D., Fengjiao Guan, Zhonghao Bai, Libo Cao, Haojie Mao, *The effect of storage time in saline solution on the material properties of cortical bone tissue.* Clinical Biomechanics 2018. **57**: p. 56-66.
55. Fischer B, K.S., Höch A, Schleifenbaum S., *The influence of different sample preparation on mechanical properties of human iliotibial tract.* Sci Rep, 2020.
56. Hammer, N., et al., *Sample size considerations in soft tissue biomechanics.* Acta Biomater, 2023. **169**: p. 168-178.

7 Attachment

The following measurement protocols contain the values measured and collected in the study. This data set was also used to calculate the results and findings results. The blank fields represent the missing measurements due to material/system failure under load.

Sample ID	Ref. area (mm2)	Failure stretch (-)	Failure load (N)	Failure Cauchy stress (N/mm^2=MPa)	E-modulus, regr. Method (N/mm^2=MPa)
K10VABL	7.96	1.68869123	5.024	1.06582723	1.84380649
L33VABL	4.88	1.72208994	40.115	14.1560733	55.2535299
L40VABL	2.23	1.61722016	2.061	1.49465953	3.04502708
L44VABL	4.67	1.91104728	8.341	3.41328594	8.03383445
L67VABL	2.88	2.02054066	3.285	2.30467919	2.6483094
L69VABL	1.12	1.45260959	6.78	8.79347593	35.9023298
L70VABL	3.62	1.44624615	9.839	3.9308331	10.8239302
L82VABL	8.15	1.82867235	3.221	0.72271824	1.21921405
L84VABL	3.14	1.6101361	2.576	1.32092694	2.47040176
L85VABL	2.27	1.33472692	1.61	0.94665654	*
M23VABL	6.12	2.35431815	0.757	0.29121223	*
K10VFBL	9.46	1.54869869	4.412	0.72228949	2.59006412
L33VFBL	8.99	1.63440395	33.238	6.04274955	14.0567142
L40VFBL	4.47	1.92433966	2.754	1.18559987	2.26280207
L44VFBL	6.57	1.47810066	2.56	0.57594181	1.31432185
L67VFBL	4.29	1.7364035	3.736	1.51216865	3.61684572
L69VFBL	5.49	1.87801673	4.123	1.41039399	3.36706044
L70VFBL	7.41	1.43078738	4.01	0.77428575	2.31816894
L82VFBL	1.65	1.68338432	3.334	3.40145655	7.24329787
L84VFBL	9.21	1.64928034	0.902	0.16152561	*
L85VFBL	3.87	1.43292315	5.443	2.01534902	10.7356209
M23VFBL	5.29	1.42375431	1.256	0.33804072	*
K10VAKK	4.01	1.3830787	12.56	4.33203703	13.8362346
L33VAKK	3.72	1.20866026	17.215	5.5933028	45.7614815
L40VAKK	2.97	1.63591504	19.986	11.0085515	36.0714742
L44VAKK	3.94	1.45849941	27.376	10.1339797	42.9148092
L67VAKK	2.35	1.68327226	0.547	0.39180848	*
L69VAKK	3.51	1.97497974	7.489	4.21385278	5.9182326
L70VAKK	3.82	1.54105617	7.73	3.11841994	9.43304735
L82VAKK	3.04	1.39360664	8.906	4.08271734	13.7991014
L84VAKK	7.29	1.78506364	5.556	1.36046825	2.08031134
L85VAKK	2.27	1.58226755	4.992	3.47959454	11.8155099
M23VAKK	2.75	1.52938435	12.401	6.89668919	17.3856626
K10VFKK	1.94	1.60166057	4.122	0.60347759	1.16641368
L33VFKK	2.96	2.49304123	1.079	0.90878091	*
L40VFKK	4.27	1.49641905	5.814	2.03751296	6.20560019
L44VFKK	15.03	1.72826112	3.913	0.44994583	0.66342215
L67VFKK	3.28	1.79776359	3.043	1.66786421	2.35282706

L69VFKK	6.28	1.49763433	3.704	0.88331808	2.35277503
L70VFKK	3.65	1.66150545	7.021	3.19600815	5.14607937
L82VFKK	5.8	1.39344915	2.85	0.68471208	1.63991201
L84VFKK	11.05	1.48401733	6.442	0.86516196	1.92233276
L85VFKK	4.65	1.70040764	6.2	2.26721018	4.20362181
M23VFKK	9.5	1.47684666	10.098	1.56981027	4.66348718

*not included since the sample did not surpass the preconditioning cycle

PEG 10% + control group

#	Proben-ID	Empty Eppendorf tube with drilled lid		Osmotic stress protocol (PEG immersion of specimens)		Eppendorf tube with frozen specimen (wet, -80°C)		Vacuum protocol, Eppendorf tube with freeze-dried specimen (dry, room temp.)		
		Date, Time	Weight (mg)	Start (date, time)	End (date, time)	Date, Time	Weight (mg)	Start (date, time)	End (date, time)	Weight (mg)
1	K10	31.01.2024, 8:00	1007,46	13.02.2024, 13:00	13.02.2024, 13:00	13.02.2024, 13:00	1027,86	14.02.2024, 09:00	16.02.2024, 13:00	1012,21
2	L33		1007,40				1030,14			1015,21
3	L44		1008,62				1035,42			1017,60
4	L40		1004,68				1014,73			1008,82
5	L67		1006,04				1022,25			1013,19
6	L69		1004,98				1023,80			1013,74
7	L70		1003,55				1035,91			1016,77
8	L84		1004,58				1024,21			1013,94
9	L85		1005,20				1022,20			1010,35
10	L82		1006,12				1018,11			1010,24
11	M23		1005,64				1022,22			1011,61
12										
13										
14										
15										
Median			**1005,64**				**1023,80**			**1013,19**
Mean			**1005,84**				**1025,17**			**1013,06**
Standard dev.			**1,42**				**6,32**			**2,63**

Determination of water content after submersion for 8 hours

#	Proben-ID	Empty Eppendorf tube with drilled lid		Osmotic stress protocol (PEG immersion of specimens)		Eppendorf tube with frozen specimen (wet, -80°C)		Vacuum protocol, Eppendorf tube with freeze-dried specimen (dry, room temp.)		
		Date, Time	Weight (mg)	Start (date, time)	End (date, time)	Date, Time	Weight (mg)	Start (date, time)	End (date, time)	Weight (mg)
1	K10	13.03.2024, 16:00	1010,65	14.03.2024, 08:00	14.03.2024, 16:00	14.03.2024, 19:00	1031,96	15.03.2024, 14:00	18.03.2024, 15:00	1014,94
2	L33		1007,11				1046,82			1026,32
3	L44		1003,67				1034,20			1011,61
4	L40		1003,70				1028,65			1008,51
5	L67		1004,71				1024,41			1007,61
6	L69		1008,16				1029,52			1013,50
7	L70		1004,70				1032,29			1012,57
8	L84		1003,73				1028,40			1008,40
9	L85		1005,89				1028,36			1011,23
10	L82		1005,27				1036,08			1009,46
11	M23		1008,55				1045,78			1022,43
12										
13										
14										
15										
Median			**1005,27**				**1031,96**			**1011,61**
Mean			**1006,01**				**1033,32**			**1013,33**
Standard dev.			**2,21**				**6,83**			**5,70**

Determination of water content after submersion for 12 hours

#	Proben-ID	Empty Eppendorf tube with drilled lid		Osmotic stress protocol (PEG immersion of specimens)		Eppendorf tube with frozen specimen (wet, -80°C)		Vacuum protocol, Eppendorf tube with freeze-dried specimen (dry, room temp.)		
		Date, Time	Weight (mg)	Start (date, time)	End (date, time)	Date, Time	Weight (mg)	Start (date, time)	End (date, time)	Weight (mg)
1	K10	13.03.2024, 16:00	1009,27	14.03.2024, 08:00	14.03.2024, 20:00	14.03.2024, 21:00	1057,23	15.03.2024, 14:00	18.03.2024, 15:00	1019,24
2	L33		1005,03				1044,22			1016,80
3	L44		1006,25				1060,09			1024,27
4	L40		1009,27				1038,69			1014,68
5	L67		1003,58				1037,58			1008,64
6	L69		1008,65				1043,50			1018,20
7	L70		1004,33				1061,90			1021,30
8	L84		1010,17				1057,10			1023,33
9	L85		1006,16				1031,48			1011,59
10	L82		1008,53				1031,80			1013,24
11	M23		1007,60				1037,63			1013,03
12										
13										
14										
15										
Median			**1007,60**				**1043,50**			**1016,80**
Mean			**1007,17**				**1045,57**			**1016,76**
Standard dev.			**2,12**				**10,93**			**4,78**

Determination of water content after submersion for 24 hours

#	Proben-ID	Empty Eppendorf tube with drilled lid		Osmotic stress protocol (PEG immersion of specimens)		Eppendorf tube with frozen specimen (wet, -80°C)		Vacuum protocol, Eppendorf tube with freeze-dried specimen (dry, room temp.)		
		Date, Time	Weight (mg)	Start (date, time)	End (date, time)	Date, Time	Weight (mg)	Start (date, time)	End (date, time)	Weight (mg)
1	K10	13.03.2024, 16:00	1005,61	13.03.2024, 16:00	14.03.2024, 16:00	14.03.2024, 19:00	1036,19	15.03.2024, 14:00	18.03.2024, 15:00	1014,61
2	L33		1009,04				1038,19			1014,58
3	L44		1004,00				1055,94			1015,71
4	L40		1007,10				1045,01			1014,01
5	L67		1005,80				1041,68			1010,71
6	L69		1007,47				1038,41			1013,06
7	L70		1004,26				1032,75			1011,89
8	L84		1006,83				1048,15			1017,07
9	L85		1006,78				1044,66			1014,15
10	L82		1003,52				1026,76			1008,50
11	M23		1009,02				1032,65			1014,18
12										
13										
14										
15										
Median			**1006,78**				**1038,41**			**1014,15**
Mean			**1006,31**				**1040,04**			**1013,50**
Standard dev.			**1,79**				**7,82**			**2,27**

PEG 5%

#	Proben-ID	Determination of water content after submersion for 8 hours								
		Empty Eppendorf tube with drilled lid		Osmotic stress protocol (PEG immersion of specimens)		Eppendorf tube with frozen specimen (wet, -80°C)		Vacuum protocol, Eppendorf tube with freeze-dried specimen (dry, room temp.)		
		Date, Time	Weight (mg)	Start (date, time)	End (date, time)	Date, Time	Weight (mg)	Start (date, time)	End (date, time)	Weight (mg)
1	K10	31.01.2024, 8:00	1007,65	12.02.2024, 11:00	12.02.2024, 19:00	13.02.2024, 13:00	1028,75	14.02.2024, 09:00	16.02.2024, 13:00	1012,27
2	L33		1006,81				1053,88			1020,17
3	L44		1010,28				1038,32			1020,03
4	L40		1004,49				1017,82			1014,92
5	L67		1008,68				1033,33			1017,49
6	L69		1003,34				1022,61			1010,18
7	L70		1008,42				1030,64			1013,10
8	L84		1001,41				1022,29			1006,94
9	L85		1005,08				1022,75			1015,55
10	L82		1006,61				1022,37			1009,95
11	M23		1008,01				1018,10			1009,87
12										
13										
14										
15										
Median			**1006,81**				**1022,75**			**1013,10**
Mean			**1006,43**				**1028,26**			**1013,68**
Standard dev.			**2,49**				**10,15**			**4,16**

#	Proben-ID	Determination of water content after submersion for 12 hours								
		Empty Eppendorf tube with drilled lid		Osmotic stress protocol (PEG immersion of specimens)		Eppendorf tube with frozen specimen (wet, -80°C)		Vacuum protocol, Eppendorf tube with freeze-dried specimen (dry, room temp.)		
		Date, Time	Weight (mg)	Start (date, time)	End (date, time)	Date, Time	Weight (mg)	Start (date, time)	End (date, time)	Weight (mg)
1	K10	31.01.2024, 8:00	1002,56	12.02.2024, 20:00	13.02.2024, 08:00	13.02.2024, 13:00	1039,90	14.02.2024, 09:00	16.02.2024, 13:00	1008,08
2	L33		1003,75				1026,29			1009,48
3	L44		1007,07				1055,28			1014,45
4	L40		1007,53				1037,08			1011,98
5	L67		1005,21				1036,41			1013,38
6	L69		1005,89				1033,13			1009,37
7	L70		1008,99				1089,11			1019,77
8	L84		1005,97				1027,82			1009,88
9	L85		1003,01				1030,60			1007,16
10	L82		1001,71				1024,27			1004,83
11	M23		1003,30				1033,89			1008,19
12										
13										
14										
15										
Median			**1005,21**				**1033,89**			**1009,48**
Mean			**1005,00**				**1039,43**			**1010,60**
Standard dev.			**2,21**				**17,63**			**3,92**

#	Proben-ID	Determination of water content after submersion for 24 hours								
		Empty Eppendorf tube with drilled lid		Osmotic stress protocol (PEG immersion of specimens)		Eppendorf tube with frozen specimen (wet, -80°C)		Vacuum protocol, Eppendorf tube with freeze-dried specimen (dry, room temp.)		
		Date, Time	Weight (mg)	Start (date, time)	End (date, time)	Date, Time	Weight (mg)	Start (date, time)	End (date, time)	Weight (mg)
1	K10	31.01.2024, 8:00	1006,49	08.02.2024, 16:00	09.02.2024, 16:00	13.02.2024, 13:00	1026,47	14.02.2024, 09:00	16.02.2024, 13:00	1012,63
2	L33		1008,13				1036,04			1015,91
3	L44		1005,45				1038,03			1014,04
4	L40		1007,11				1018,19			1010,74
5	L67		1008,97				1038,57			1017,60
6	L69		1006,41				1023,98			1012,59
7	L70		1003,74				1022,72			1011,94
8	L84		1003,87				1014,31			1007,10
9	L85		1005,12				1029,90			1011,58
10	L82		1006,57				1030,20			1017,20
11	M23		1003,54				1021,28			1011,98
12										
13										
14										
15										
Median			**1006,41**				**1026,47**			**1012,59**
Mean			**1005,95**				**1027,24**			**1013,03**
Standard dev.			**1,71**				**7,71**			**2,90**

PEG 2.5%

#	Proben-ID	Determination of water content after submersion for 8 hours								
		Empty Eppendorf tube with drilled lid		Osmotic stress protocol (PEG immersion of specimens)		Eppendorf tube with frozen specimen (wet, -80°C)		Vacuum protocol, Eppendorf tube with freeze-dried specimen (dry, room temp.)		
		Date, Time	Weight (mg)	Start (date, time)	End (date, time)	Date, Time	Weight (mg)	Start (date, time)	End (date, time)	Weight (mg)
1	K10	26.03.2024, 16:00	1005,97	27.03.2024, 07:30	27.03.2024, 15:30	27.03.2024, 19:00	1043,21	02.04.2024, 15:00	05.04.2024, 09:00	1012,78
2	L33		1005,91				1058,89			1024,73
3	L44		1007,99				1043,57			1013,28
4	L40		1003,29				1054,88			1006,56
5	L67		1005,76				1037,55			1009,06
6	L69		1005,03				1020,84			1007,28
7	L70		1010,89				1054,45			1025,04
8	L84		1002,96				1028,73			1009,70
9	L85		1006,95				1040,49			1013,03
10	L82		1008,39				1058,03			1012,26
11	M23		1005,48				1049,65			1009,78
12										
13										
14										
15										
Median			**1005,91**				**1043,57**			**1012,26**
Mean			**1006,24**				**1044,57**			**1013,05**
Standard dev.			**2,17**				**11,67**			**5,99**

#	Proben-ID	Determination of water content after submersion for 12 hours								
		Empty Eppendorf tube with drilled lid		Osmotic stress protocol (PEG immersion of specimens)		Eppendorf tube with frozen specimen (wet, -80°C)		Vacuum protocol, Eppendorf tube with freeze-dried specimen (dry, room temp.)		
		Date, Time	Weight (mg)	Start (date, time)	End (date, time)	Date, Time	Weight (mg)	Start (date, time)	End (date, time)	Weight (mg)
1	K10	26.03.2024, 16:00	1011,67	27.03.2024, 07:30	27.03.2024, 19:30	02.04.2024, 14:00	1030,02	02.04.2024, 15:00	05.04.2024, 09:00	1013,99
2	L33		1010,73				1049,45			1024,37
3	L44		1001,95				1025,74			1003,99
4	L40		1006,18				1043,63			1012,82
5	L67		1004,34				1036,32			1011,77
6	L69		1007,59				1031,32			1009,62
7	L70		1005,31				1028,03			1011,61
8	L84		1007,03				1103,79			1020,84
9	L85		1007,21				1038,37			1012,77
10	L82		1005,81				1035,39			1012,56
11	M23		1009,58				1072,45			1024,10
12										
13										
14										
15										
Median			**1007,03**				**1036,32**			**1012,77**
Mean			**1007,04**				**1044,96**			**1014,40**
Standard dev.			**2,70**				**22,39**			**5,95**

#	Proben-ID	Determination of water content after submersion for 24 hours								
		Empty Eppendorf tube with drilled lid		Osmotic stress protocol (PEG immersion of specimens)		Eppendorf tube with frozen specimen (wet, -80°C)		Vacuum protocol, Eppendorf tube with freeze-dried specimen (dry, room temp.)		
		Date, Time	Weight (mg)	Start (date, time)	End (date, time)	Date, Time	Weight (mg)	Start (date, time)	End (date, time)	Weight (mg)
1	K10	26.03.2024, 16:00	1004,14	26.03.2024, 17:00	27.03.2024, 17:00	27.03.2024, 19:00	1043,17	02.04.2024, 15:00	05.04.2024, 09:00	1010,98
2	L33		1002,86				1046,80			1014,16
3	L44		1007,50				1033,72			1013,22
4	L40		1007,80				1036,73			1011,79
5	L67		1005,72				1039,19			1011,96
6	L69		1009,07				1046,09			1013,87
7	L70		1003,85				1054,03			1015,71
8	L84		1001,93				1030,08			1014,53
9	L85		1007,07				1066,46			1017,42
10	L82		1006,15				1028,01			1010,25
11	M23		1003,37				1033,19			1009,68
12										
13										
14										
15										
Median			**1005,72**				**1039,19**			**1013,22**
Mean			**1005,41**				**1041,59**			**1013,05**
Standard dev.			**2,21**				**10,88**			**2,27**